2010

Evaluation of hydro-mechanical pulsation for rocket injector research

Matthew B. Wilson

EVALUATION OF HYDRO-MECHANICAL PULSATION FOR ROCKET INJECTOR RESEARCH

by

MATTHEW B. WILSON

A THESIS

Submitted in partial fulfillment of the requirements
for the degree of Master of Science in Engineering
in
The Department of Mechanical and Aerospace Engineering
to
The School of Graduate Studies
of
The University of Alabama in Huntsville

HUNTSVILLE, ALABAMA

2010

In presenting this thesis in partial fulfillment of the requirements for a master's degree from The University of Alabama in Huntsville, I agree that the Library of this University shall make it freely available for inspection. I further agree that permission for extensive copying for scholarly purposes may be granted by my advisor or, in his/her absence, by the Chair of the Department or the Dean of the School of Graduate Studies. It is also understood that due recognition shall be given to me and to The University of Alabama in Huntsville in any scholarly use which may be made of any material in this thesis.

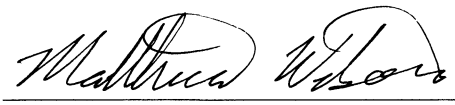

Matthew B. Wilson

10/21/2010
(date)

THESIS APPROVAL FORM

Submitted by Matthew B. Wilson in partial fulfillment of the requirements for the degree of Master of Science in Engineering in Mechanical Engineering and accepted on behalf of the Faculty of the School of Graduate Studies by the thesis committee.

We, the undersigned members of the Graduate Faculty of The University of Alabama in Huntsville, certify that we have advised and/or supervised the candidate of the work described in this thesis. We further certify that we have reviewed the thesis manuscript and approve it in partial fulfillment of the requirements for the degree of Master of Science in Engineering in Mechanical Engineering.

Marlow D Moser 13 Oct 2010 Committee Chair
Dr. Marlow D. Moser (Date)

10/20/2010
Dr. David M. Lineberry (Date)

10/21/2010
Dr. M. S. Balasubramanyam (Date)

10/27/10 Department Chair
Dr. Kader Frendi (Date)

10/27/10 College Dean
Dr. Shankar Mahalingam (Date)

12/2/10 Graduate Dean
Dr. Rhonda K. Gaede (Date)

ABSTRACT

School of Graduate Studies
The University of Alabama in Huntsville

Degree Masters of Science in Engineering College/Dept. Engineering/Mechanical and Aerospace Engineering

Name of Candidate Matthew B. Wilson

Title Three-Dimensional Numerical Modeling of a Diagonal Magnetohydrodynamic Accelerator

The Propulsion Research Center at the University of Alabama in Huntsville has designed and built a hydro-mechanical pulsator to simulate the pressure fluctuations created by high frequency combustion instability. The pressure response characteristics were evaluated in an atmospheric test rig using filtered de-ionized water as the working fluid. The outlet of the pulsator was connected to a swirl injector post to provide downstream flow resistance. Previous low pressure and mass flow experimental data revealed a complex relationship between the control parameters and the pulsation response. For each test, the average mass flow rates of the waste water, water lost through the seals, and injector mass flow rates are measured. A dynamic pressure transducer at the pulsator exit measures and records the pressure waveform. Pulsation magnitude, reliability, repeatability, pulsation effects, and detailed variable control are examined. The data shows the pulsator is capable of generating 30% pulsation at 1575 Hz input. The repeatability of the pulsator is questionable because the standard deviations exceeded 40% of the average. The detailed data obtained during this research provides is sufficient to develop a pulsator tuning procedure for future applications.

Abstract Approval: Committee Chair

Dr. Marlow D. Moser

Department Chair

Dr. Kader Frendi

Graduate Dean

Dr. Rhonda K. Gaede

ACKNOWLEDGMENTS

I would like to begin by thanking my Advisor and Committee Chair, Dr. Morlow Moser. I would like to thank Dr. David Lineberry and Dr. M.S. Balasubramanyam for serving on my committee, providing excellent feedback, and attention to detail. Dr. David Lineberry deserves a special thanks for always being around available when no one else was around and answering or working through issues. To Dr. Kader Frendi and Dr. Robert Frederick, I thank them for their work in funding my time at UAhuntsville both through their research grants and teaching assistantships. I would also like to thank Chad Eberhart who has spent far more time on getting the spray facility operational longer than I have.

Their have been several family members who have encouraged me, but have also directly help me finish my thesis that I would like to thank. I would like to first thank my father, David Wilson, who has help solve and address several issues with his electrical experience. My grandmother, Ann Long, has helped me financially and Jorj Long who spent several long nights proofreading my thesis to get it to my committee quickly.

TABLE OF CONTENTS

PAGE

List of Figures **x**

List of Tables **xii**

Chapter

1 Introduction **1**

1.1 Background 1

1.2 Literature Review 2

1.2.1 Review of Combustion Instability 2

1.2.1.1 Combustion Instability Classifications 4

1.2.1.2 Experimental Methods 6

1.2.2 Overview of Cold Flow Testing 8

1.2.3 Review of Pulsation Devices 9

1.3 Summary and Problem Statement 14

2 Experimental Approach **17**

2.1 Overview 17

2.2 Pulsator Development 18

2.3 Pulsator Hydraulics 19

2.4 Test Facility 21

2.4.1 Test Instrumentation and Data Acquisition 24
2.5 Test Parameters and Matrix 26
2.5.1 Low Pressure Testing 27
2.5.2 High Pressure Pulsation Verification 29
2.5.3 Repeatability Testing 30
2.5.4 Position Testing 32
2.5.5 General Characterization 35
2.6 Data Processing 35
2.7 Uncertainty and Assumption Summary 37

3 Experimental Results **39**

3.1 Pulsation 39
3.2 Repeatability 43
3.3 Pulsation in System 48
3.4 Low Pressure Characterization 51
3.4.1 Initial Pressure Control 52
3.4.2 Frequency Control 52
3.4.3 Orifice Throttle Control 54
3.4.4 Back Pressure Throttle Control 59
3.5 High Pressure Characterization 64
3.5.1 Orifice Throttle Control 65
3.5.2 Back Pressure Throttle Control 68
3.6 Pulsator Tuning 74

4 Conclusions **76**

4.1 Continuing and Future Work 77

APPENDIX A: Data Summary Tables **80**

APPENDIX B: MATLAB Code **85**

REFERENCES **92**

LIST OF FIGURES

FIGURE PAGE

1.1 Working mechanism for the Seoul feed line pulsator. [1] 11

1.2 Transient waves with time by the DPMM in the pulsating state. The mean injection pressure is 3 bar (44 psi) and pressure fluctuation frequency is 5 Hz. a)The pressure measured in the manifold, b) the pressure and film thickness measured in the orifice, the calculated axial velocity, and the DPMM calculated mass flow rate through the orifice [1] 12

1.3 Schematic drawing of swirl injector pulator: Right - a)shaft, b)vanes, c)swirl chamber, d)injector inlet cap, e)dynamic inlet cap, f)manifold cap, g)manifold, h)bearings, i)water supply inlet cap, j)pressure transducer tap 1, k)pressure transducer tap 2. Left - View of cross section at A-A, where holes on rotating inlet cap and injector channels are aligned. [2] 14

2.1 Cross section of the PRC pulsator: 1) Driveshaft, 2) Case, 3) Rotating Disk, 4) Orifices, 5) Check valve, 6) Outlet to injector, 7) Diverter chamber, 8) Orifice throttle, 9) Inlet, 10) Teflon seal, 11) Drainage outlet, 12) Drainage cavity, 13) Weep outlet. The back pressure throttle is needle valve down stream of 11. 20

2.2 Floor plan of the PRC spray facility. 23

2.3 A side view representation of the PRC spray facility. 24

2.4 An example of Matlab code output. 37

3.1 Comparison of dynamic transducer data with the pulsator On and Off. A) Waveform with pulsation B) FFT with pulsation C)Waveform without pulsation D) FFT without pulsation 40

3.2 Images from the high speed video A)2100 Hz Pulsed Flow B) No Pulsation C) 105 Hz Pulsed Flow. 41

3.3 The pulsation magnitude is graphed against position. The x axis is not representative of the distance from the pulsator. 49

3.4 The graph includes a waveform section and the FFT frequency results down stream of the venturi. 49

3.5 Comparison of flow response from high frequency pressure transducer at low pressure. 53

3.6 Effect of the orifice throttle on injector pressure. 55

3.7 Effect of the orifice throttle on injector mass flow. 57

3.8 Effect of the orifice throttle on percent pulsation. 58

3.9 Effect of the back pressure throttle on injector pressure. 60

3.10 Effect of the back pressure throttle on injector mass flow. 61

3.11 Effect of the back pressure throttle on injector mass flow fraction. . . 62

3.12 Effect of the back pressure throttle on percent pulsation. 63

3.13 Effect of the orifice throttle on injector pressure. 66

3.14 Effect of the orifice throttle on injector mass flow 67

3.15 Effect of the orifice throttle on percent pulsation. 68

3.16 Effect of the back pressure throttle on injector pressure. 69

3.17 Relationship between the feedline pressure and the injector mass flow rate. 70

3.18 Effect of the back pressure throttle on injector mass flow rate. 70

3.19 Effect of the back pressure throttle on injector mass flow fraction. . . 71

3.20 Effect of the back pressure throttle on percent pulsation. 72

3.21 Effect of the back pressure throttle on percent pulsation. 73

LIST OF TABLES

TABLE PAGE

2.1 Pulsator Types Advantages and Disadvantages 18

2.2 Low Pressure Characterization Set Points 28

2.3 Repeatability Test Summary 30

2.4 Repeatability Test Set Points 30

2.5 High Pressure Characterization Set Points 34

3.1 On/Off Repeatability Results Summary 44

3.2 2100 Hz Throttle Repeatability Set Point Summary 45

3.3 Corrected 2100 Hz Throttle Repeatability Set Point Summary 46

3.4 1575 Hz Throttle Repeatability Set Point Summary 47

3.5 Pulsation Threshold Table 47

A.1 Data Recorded During the Tests 81

A.2 Mass Flow Calculations 82

A.3 System Pressure Values 83

A.4 Data Relating to Pulsator Operation 84

To my grandfather, G. G. Long

If we knew what it was we were doing, it would not be called research, would it?

—Albert Einstein

CHAPTER 1

INTRODUCTION

If you want to understand today,
you have to search yesterday.

—Pearl Buck

1.1 Background

Rocket propulsion system development includes resolving many problems. The most common, hazardous, and difficult to resolve is combustion instability. Nearly every rocket engine has experienced combustion instability problems. These problems drastically slow down and increase the cost of engine development, consequently there is considerable need to increase the understanding of combustion instability [3]. The continued unresolved complexities of the physical and chemical mechanisms have resulted in a design process that does not focus on eliminating instability during the design process. Instead, instability is addressed when it appears in the testing of new systems. There are existing proven corrective procedures; however, these procedures are really a guided guess and check process developed from solving previous engine instabilities [3]. The Saturn F-1 engine underwent the largest test program to solve its combustion instabilities. The F-1 engine was subjected to 2,700 full-scale tests to understand and solve its instabilities [4].

The most visible issue with combustion instability is engine and rocket failure and the resulting risk to humans. With the current safety precautions that are in place the primary issue is maintaining the budget and resource constraints on current and future projects. The primary method to resolve combustion instability is to change the injector design, layout, or baffle placement, then retest the rocket engine [3]. The process of fixing the F-1 engine resulted in more than 2,700 full-scale tests. The Ares I booster thrust variations and vibration problems were solved, and the upcoming 2011 President's Budget cancels the Constellation program including the Ares I booster. The vibration problems are not specifically cited for the cancellation; however, the rising cost and delays contributed to the programs demise [5]. In the present environment, the complications of solving combustion system problems with traditional methods are unacceptable for completing a new motor design. Sub scale testing and basic research provide a more affordable option for studying and eliminating combustion instability early in the engine design process.

1.2 Literature Review

1.2.1 Review of Combustion Instability

Combustion instability results from the coupling between the combustion and fluid dynamics of the system. The coupling enables the combustion to supply oscillatory energy. Depending on the magnitude of the damping processes, the oscillatory energy dissipates or builds. When the oscillatory energy builds, it results in combustion instabilities. Instability manifests itself in many different ways. The most

effective detection method is combustion chamber pressure measurements. Pressure oscillations in the combustion chamber range from 100 to 15,000 hertz with amplitudes from up to 1000 percent of the designed chamber pressure [3]. Instabilities are also detected by vibration measurements; however, vibration measurements do not correlate well with corresponding chamber pressure measurements. Frequently, there are similarities in frequency and severity or amplitude making vibration an acceptable detection method, but not a good diagnostic method. It is possible to use non flow intrusive optical techniques to detect combustion instability in the plumes or shock diamonds, but the changes are small compared to the magnitude of pressure and vibration [3].

Combustion instability is known for causing engine failure and unpredictable behaviour. Combustion instability damage is produced by physical stress and the changing conditions within the combustion chamber. Engines experience different failure modes under the stress of combustion instability. One particular engine's instability resulted in physical stress that manifested with the severing off the nozzle at the throat [3]. A form of secondary damage occurs when pressure waves change the heat transfer rate to the chamber wall and injector face causing the failure of the chamber, injectors, or both. Instability is not always dramatically, destructive; low frequency modes may not do any damage and the amplitude at high frequencies may be low enough that damage goes undetected over short tests. High frequency instability modes may require a sophisticated set of instrumentation to determine if combustion is unstable during short tests [3].

Empirical combustion stability data demonstrates that combustion instability often increases engine performance. Nevertheless to compensate for the instability, the engines must be redesigned. This apparent increase in performance actually represents non-optimally designed injectors and injector configurations [6]. Combustion instabilities create high transverse pressure and velocity gradients that enhance mixing and vaporization, both factors that improve engine performance. High frequency combustion instability in rocket engines with optimally designed injectors result in localized variations in the mixture reducing combustion efficiently. In poor engine designs that are not naturally high performers, the high frequency instabilities tend to increase combustion efficiency [3].

1.2.1.1 Combustion Instability Classifications

Historically combustion instability classification has only been based on frequency, but a better method is to examine the effects and the coupling mechanisms involved [3].Combustion instability is classified into three primary types. As a generalization there is low, intermediate, and high frequency combustion instabilities. Low frequency combustion is known as chug, pogo, or putt-putt, and is, characterized by a coupling between the feed system and the combustion process, and has a frequency range of 100 to 400 Hertz. It occurs more frequently at low chamber pressures, 100 to 500 psi [7]. Out of all the type of instabilities, chug has the best models for predicting and finding a solution for the instability. The most frequent solution is to use an accumulator in the feed lines to dampen the pressure waves; additional measures such

as increasing the injector pressure drop, injector length to diameter ratio, or reducing chamber size may be required to reduce or prevent the coupling from occurring [3].

Intermediate frequency is known as buzzing. This category is primarily a catch group for instabilities between the two extreme types with a frequency range of 400 to 1000 Hertz [7]. One of the disadvantages of using frequency to classify instabilities results in incorrect classification. Chug instabilities with frequencies higher than traditional range are often classified as buzz when focusing on frequency and not the underlying coupling. The shape of the buzzing pressure waves are nearly sinusoidal and can be found in one or both of the propellant feed systems. Buzz type instabilities are not particularly damaging, but may reduce engine performance or trigger high frequency instability [3].

High frequency instability is also known as screeching, screaming, acoustic, or resonant combustion instability. High frequency is the most destructive type of instability occurring over 1000 hertz. The high frequency combustion instability is caused by resonates in the combustion chamber and is weakly dependent on the feed line system. Each wave affects the combustion process enough to supply sustaining energy to the chamber [7]. The instabilities can be resolved by changing the injector pattern, baffle arrangement, or acoustic cavities. The relationship between the changes and the stabilization is not well known, only general tendencies have been observed. The tendencies then lead to trial and error methods to reduce combustion instability [3].

1.2.1.2 Experimental Methods

Normally two methods are used to study combustion instability in liquid rocket engines. The first method is simulation and modeling. Simulations and modeling are dependent on the data from previous rocket engine tests and newer computer capabilities to create models of the underlining physics. An example of this type of modelling is the use of computational fluid dynamics (CFD). CFD uses the availability of fast cheap computing power available to attempt to predict injection-coupled combustion stability behavior. Models are used to predict may aspects of the rocket engines. CFD is in injector behavior, engine vehicle interactions, heat transfer analysis, and thruster design. CFD models and analysis processes require verification to be fully implemented in design processes.

The second method is experimental and is divided in to sub-categories including full-scale, components, and laboratory-scale experimental methods. Full scale testing has the simplest type of testing setup. It utilizes a full size rocket engine under similar conditions the engine is expected to experience when used as part of the finished vehicle. Results from these tests have the highest accuracy and reliability, but require immense resources for large engines. Testing in this fashion requires the most amount of work to change and refine the design if problems are detected. Although full scale testing produces the best results, it is the most difficult to execute and obtain the large amounts of funding necessary [8]. Full-scale tests are frequently part of the system test. At this point, the focus has shifted from a primary investigative tool to a late full system stage check out. Often times enough testing and

simulations have been done prior to this stage of development so that there are few or no issues from the full scale testing to resolve. Cost, environmental, and safety issues have reduced the number of full scale tests scheduled in new engine development programs.

Component testing uses full-scale parts of rocket engines. Testing the individual engine components identifies the impact the particular part has on combustion instability. The results for component testing typically agree with the full-scale because of the use of full-scale part in the test. One of the primary short comings of component methodology is the failure to show the interactions between individual parts. Despite reducing the system to individual elements, the tests demonstrate the combustion interactions present. The primary advantage is the cost reduction of the testing. In addition, the testing can be performed as the individual part designs are completed rather than waiting until the engine is finished to perform testing. Component testing can successfully be implemented to reduce the problems discovered in the final engine design, by allowing tests to be done for lower cost and as the individual parts are completed [3].

Laboratory-scale testing is most advantageous from a cost perspective, but requires the most up front analysis to match non-dimensional scaling parameters. The scaling parameters must then be also taken into account when looking at the results and effects on the full scale parts. There are many approaches to sub-scale testing. The various methods are often named after the university or location where the test were performed. The different methods focus on different scaling parameters and how to effectively match the desired scaling parameters. There are also differences in test

procedures and facilities used. Sub-scale testing allows for extensive cost effective testing that can be executed at smaller facilities [9].

1.2.2 Overview of Cold Flow Testing

Cold flow spray testing is used to understand and examine how particular injectors or rocket engine parts work without the combustion processes. The combustion processes dominate the time scale and prevent the examination of the direct output of rocket engine elements. The tests can be performed with the oxidizer and fuel without igniting the two, but most of the time simulants are used in their place. Working fluids are chosen to match the characteristics of actual propellants. Water is often chosen as the working fluid to match the density of liquid oxygen. The difference between liquid oxygen's and water's surface tension reduces the similarities in the spray break up results. To better match surface tension and viscosity values, some test facilities are capable of running tests with cryogenic simulants like LN2. Water is an acceptable simulant, as long as testing is limited to the features that are dominated by the density of the fluid [10].

The use of cold flow analysis is an important first step because engines are based on fluid mechanic considerations. Injector analysis examines several factors, including spray distribution, mixing efficiency, sheet atomization process, atomization, and sheet breakup. Images, droplet size, and velocity data are used to ascertain injector effectiveness. The cold flow data can be used to help predict hot fire performance. Variations in the spray can induce combustion instability [10]. Tests can verify if spray variations are present that could cause instabilities or regions of dif-

ferent burn rates. The cold flow investigation of injectors determines if the injectors functioned per design specifications. Cold flow test data provides insight to the hot fire results. Because combustion effects and the differences in fluid properties between the working fluids and the propellants, the data does not directly match the injector design parameters. The tests can provide insight as to how injector dynamics work and data provides the ability to improve injector design [11].

1.2.3 Review of Pulsation Devices

As previously noted cold flow testing provides the ability to examine spray dynamics. An extension of traditional cold flow testing is simulating combustion instability spray dynamics. Two primary methods have been used to try to create the effects of combustion instabilities, acoustic chamber pulsation and feed line pulsation.

Acoustic chamber pulsation uses a moving diaphragm to generate sound waves in the combustion chamber to simulate transverse waves. Acoustic pulsation primarily analyzes the effect acoustic waves have on the breakup of the spray from an injector. The technique has been used with both swirling conical sheets and flat sheets [11]. The acoustic pulsation provides a way to simulate the effect that the velocities impart on the spray from the instabilities in a rocket engine without, generating the large pressure pulsations experimentally measured in unstable engines. The similarity in the effects of acoustic pulsation and transverse steady gas flow establishes acoustic pulsation ability to reproduce the velocity field [12]. Acoustic disturbances or pulsations can drive sprays at frequencies other than the natural frequencies of the spray. The pulsation can drive the spray to near disintegration [13].

Research at the Air Force Research Laboratory has concluded, using cryogenic supercritical nitrogen flows to match LOX properties, that the sheet break up lengths are shortened by acoustic vibration [14]. Shortened break up lengths increase the destructiveness of the combustion instability if the instability is a function of how close the energy release is to the injectors [3]. The Air Force Research Laboratory has confirmed earlier work demonstrating that increased sheet and jet velocities reduce the effects of acoustic waves liquid sprays [13, 15]. The work done with acoustic pulsation has led to the development of factors that can increase spray effectiveness, but fail to synthesize the large pulsations in chamber pressure. The highest magnitude acoustic driven pulsators generate is 150 db or less than 0.1 psi which is far below the 25 psi or 5% pulsation in 500 psi combustion chamber [11].

Hydro-mechanical pulsators use a rotating valve to quickly divert or turn on and off flow. This action causes pressure pulsations in the feed lines. The first devices developed were referred to as sirens. The sirens were used in conjunction with full scale rocket engine elements, and would work with flows over 150 lb/s of water. The first pulsation devices were successful and could generate pressure oscillations with amplitudes in excess of 200 psi and frequencies up to 200 Hz. Unfortunately, the excessive vibrations lead to structural failures. The goal of the first pulsation devices was to investigate the effects of continuous feed-system disturbances, and evaluate the dynamic response of feed systems [3]. Following the development of the first synthetic pulsation systems, little has been done with the testing method during ensuing decades. Since 2000 there has been an increase in the interest in using

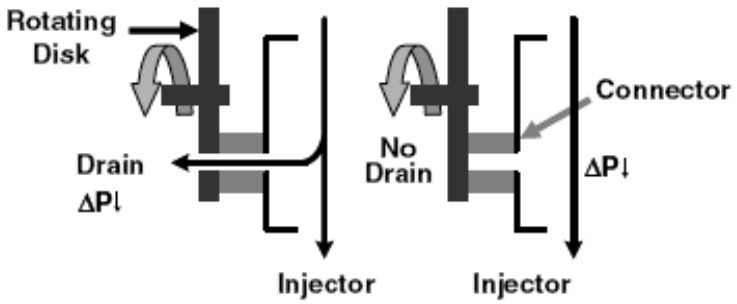

Figure 1.1: Working mechanism for the Seoul feed line pulsator. [1]

synthetic pulsation as a combustion instability investigation technique, with Purdue University and Seoul National University building hydro-mechanical pulsators [1, 2].

The Seoul National University pulsator was designed to generate pressure fluctuations in the feedlines leading to the injector; the pulsator is independent from the injector. The internal mechanics of the pulsator rely on 2 internal parts: a rotating disk and a matching connector. As shown Figure 1.1 when the hole in the rotating disk and the connector line up, a portion of the working fluid is diverted causing the pressure to drop. A motor is attached to the rotating disk. By controlling the motor's angular velocity, the rate of hole alignment or pulsation frequency is controlled. There are several different rotating disks, each with a different number of holes; by changing out the disks, the frequency range of the pulsator changes. The Seoul National University pulsator has 4 different disks that provide a total frequency range of 5 to 300 Hz.

This pulsator was used to evaluate the accuracy of planar liquid laser induced fluorescence (PLLIF) to measure mass flow rate at low frequency pulsation and steady flow. The mass flow calculated from the axial velocity and liquid film thickness is mea-

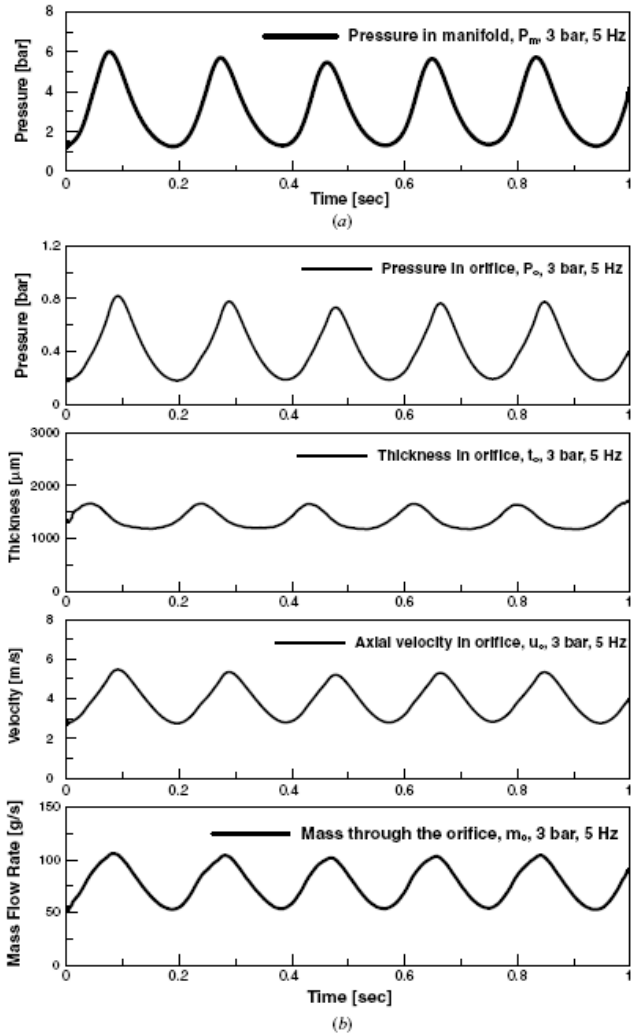

Figure 1.2: Transient waves with time by the DPMM in the pulsating state. The mean injection pressure is 3 bar (44 psi) and pressure fluctuation frequency is 5 Hz. a)The pressure measured in the manifold, b) the pressure and film thickness measured in the orifice, the calculated axial velocity, and the DPMM calculated mass flow rate through the orifice [1]

sured by electric conductance or the direct pressure measurement method (DPMM) in a fashion similar to the way the axial velocity is measured. PLLIF has been found to be accurate for frequencies below 15 Hz and DPMM has an error less than 3.0 percent over frequencies up to 300 Hz. An example data set from the Seoul pulsator experiments is presented in Figure 1.2. Note that the peak to peak pulsation produced during the test is 100% of the 3 bar or 44 psi mean injector manifold pressure. The results from the test show a clear way to provide pulsation to the injector system [1].

The Purdue University pulsator uses a rotation cylinder between the injector and the injector manifold to turn flow on and off to the injector. Figure 1.3 is the cross section of the injector and pulsation device. The outer cylinder or dynamic injector cap is rotated by a shaft connected to an electric motor outside of the injector manifold. As the injector cap is rotated, the tangential channels in the cap align with the injector's tangential channels. As the tangential channel's alignment changes, the water flow increases and decreases as the flow area changes. The injector cap can be changed to increase the pulsation frequency range. Purdue's test uses an 8 channel and 16 channel inlet cap and is stated to have a pulsation range of 100 to 3600 Hz with a 48 channel inlet cap. The tests focused on the effects of pulsation on the air core diameter and spray angle of a swirl injector.

Purdue's testing was preformed between frequencies 10 Hz to 700 Hz. The testing required two different rotating injector caps to cover the entire frequency range, an 8 channel and a 16 channel injector cap. The first set of testing covers 10 Hz to 300 Hz using a single injector cap. Tests indicated that pressure measured in the manifold experiences a sinusoidal presser fluctuation with a magnitude of 12%

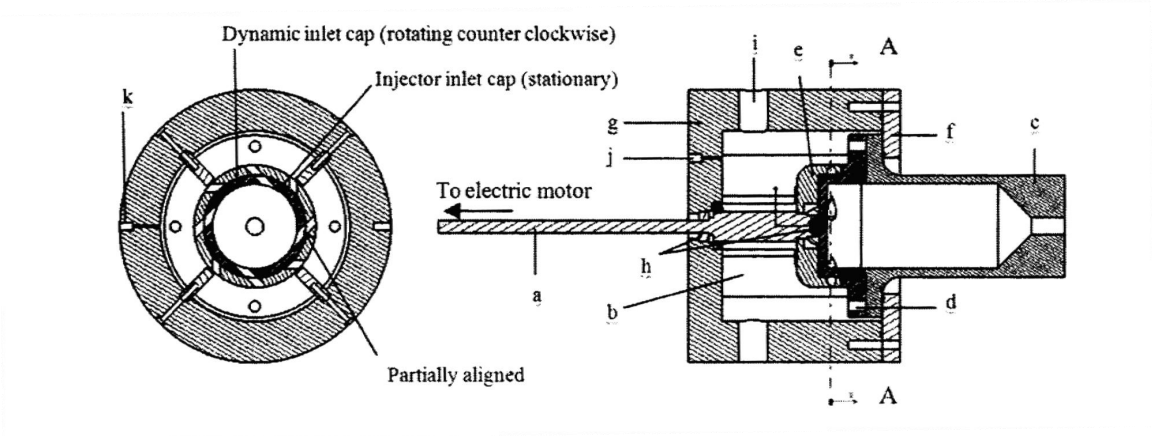

Figure 1.3: Schematic drawing of swirl injector pulator: Right - a)shaft, b)vanes, c)swirl chamber, d)injector inlet cap, e)dynamic inlet cap, f)manifold cap, g)manifold, h)bearings, i)water supply inlet cap, j)pressure transducer tap 1, k)pressure transducer tap 2. Left - View of cross section at A-A, where holes on rotating inlet cap and injector channels are aligned. [2]

at 14 Hz and drops to less than 2% above 75 Hz. The change in air core diameter is 15% at 14 psi. The air core diameter fluctuation drops and remains at close to 4% above 100 Hz. The spray angle has a maximum change of 7%, then drops to and remains near 2%. The testing above 300 Hz shows that the pulsation magnitude continues to drop with the pulsation frequency. It was noted that due to some injector and housing issues, the highest pressure tested was 55 psi [2].

1.3 Summary and Problem Statement

The results of the literature review and current status of synthetic pulsation for use in studying rocket injectors is summarized below.

What we know:

- Liquid rocket engines experience combustion instabilities which result in large variations in pressure.
- Chamber pressure oscillations occur over a wide range of frequencies.
- Air core diameter and spray angle in swirl injectors are a function of pressure drop and changes with pressure oscillations.
- Mass flow changes from artificial pulsation can be measured.
- Low frequency synthetic pressure pulsation is close to sinusoidal.
- Synthetic pulsation has achieved a 100% peak to peak pulsation at 44 psi at 5 Hz.

What we do not know:

- How will increasing the pulsation frequency impact magnitude?
- Can sufficient mean mass flow be supplied to the injector?
- Will injectors respond the same way to low and high frequency?

The study of injectors under synthetic pulsation has led to the determination of the parameters to reduce the effects of pressure and velocity from the transverse waves in the combustion chamber. The acoustic pulsations primarily have been of the effects the velocity field has on the spray. The pressure pulsation in the feed lines and the manifold structure is used to investigate the effects of the pressure pulsations

including changes in velocity and mass flow rates. The tests with hydro-mechanical pulsation have not yielded frequencies that are as high as the frequencies associated with the high frequency combustion instability. In addition to producing the high frequencies, it will also require the ability to produce adequate pulsation magnitude and mean mass flow rate to the injector.

CHAPTER 2

EXPERIMENTAL APPROACH

The true method of knowledge is experiment.

—William Blake

2.1 Overview

The goal of this research is to evaluate the PRC pulsator performance and to determine its capabilities for future integration into small scale rocket engine testing. Before starting experimentation, a literature review was conducted to guide the formation of the test matrix and the desired pulsator capabilities. The test focused on two parameters: control and characterization. In order to be able to gain an understanding of the pulsator performance, the input and control parameters were adjusted to evaluate the pulsator behavior and response. The tests included changing the three controls on the pulsator: motor angular velocity, flow to the rotating orifice, and waste water back pressure. During initial testing, the working fluid was driven by pressure only; during primary testing, the working fluid was driven by pressure and controlled using a cavitating venturi. The test was used to provide validation and an implementation methodology for the pulsator in future tests.

Table 2.1: Pulsator Types Advantages and Disadvantages

Pulsator Type	Advantages	Disadvantages
Hydro-mechanical	Low power drive	Non-Harmonic pulsation
	High pulsation amplitude	Wasted working fluid
	High pulsation frequency	Possible leaks
	Pulsation in compressible fluids	High friction
		High speed rotation
	Continuous frequency control	No Cryogenics, toxic, or hypergolic liquids
Acoustic	Harmonic pulsation	Low pulsation amplitude
	Usable with any liquid	Frequency fixed by actuator
	High pulsation frequency	High power drive
		Primarily for small scale experiments
Inertial	No leaks	High power drive
	No friction	Drive power limits amplitude
	Wide frequency range	
	Usable with any liquid	

2.2 Pulsator Development

The PRC at UAHuntsville designed and fabricated a hydro-mechanical pulsator for injector dynamic response characterization. The development of the PRC pulsator began with an analysis of different pulsation generators and how effective the designs were in small proto-type settings. The evaluation process began with investigations into hydro-mechanical, acoustic, and inertial pulsators. Each system was evaluated and the results are summarized in Table 2.1. A hydro-mechanical pulsator designe was chosen and built by Dr. Bazarov of the Moscow Aviation Institute during his stint as a visiting scholar at UAHuntsville. Heretofore pulsators focused

on lower frequencies. This pulsator was specifically designed to operate in the high frequency range from 1500 to 2100 Hz.

2.3 Pulsator Hydraulics

A cross section of the pulsator is presented in Figure 2.1 with key parts tagged by numbered callouts that are identified in the caption. The pulsator operates by having working fluid enter through the inlet pipe (9) and continue to the orifice throttling cavity (7) and then out the output line (6) where high frequency and mean pressure transducers make pressure measurements. The pulsation is created by the working fluid passing through the rotating orifice plate/disk (3). The pulsation magnitude is controled by lowering a pintle (8) to block the entrance to the orifice connection to the low pressure rotating valve side (12).

The orifice disk has 21 equal spaced circular orifices (4); the distance between the orifices on the plate must be at least the diameter of the orifices. If the spacing between orifices is too small, the volume of waste fluid increases and the pulsation amplitude is reduced because the flow is not fully cut off. Also, to maintain maximum pulsation and minimize fluid waste, the gap between the orifice disk and the connection orifice must be kept as small as possible. In Figure 2.1, the cross section of the PRC pulsator, a teflon (10) is used to form a seal between the throttle and the orifice disk. Although not included in the drawing, a spring is used to press the teflon against the rotating orifice plate. A pressurized air line can be attached to a check valve (5). Pressurizing the low pressure side with air reduces cavitation, by raising the pressure. This approach was not adopted for these pulsator experiments.

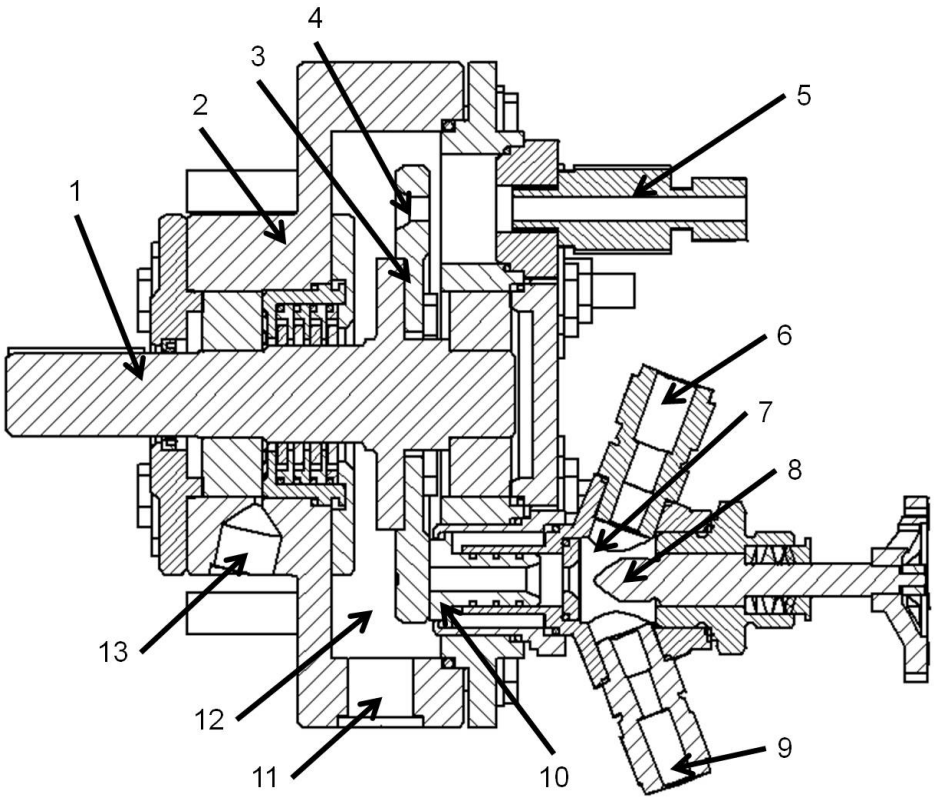

Figure 2.1: Cross section of the PRC pulsator: 1) Driveshaft, 2) Case, 3) Rotating Disk, 4) Orifices, 5) Check valve, 6) Outlet to injector, 7) Diverter chamber, 8) Orifice throttle, 9) Inlet, 10) Teflon seal, 11) Drainage outlet, 12) Drainage cavity, 13) Weep outlet. The back pressure throttle is needle valve down stream of 11.

Cavitation was controlled during testing by a needle valve on the waste discharge line that is attached to the drainage outlet (11). By adding resistance to the waste discharge line, the back pressure on the discharge side was increased. By increasing the back pressure, both the pulsation magnitude and the amount of waste working fluid can be reduced.

When pressurized working fluid is supplied to the inlet pipe line (9), pulsation can be created by temporally diverting part of the fluid flow. The liquid in the diverter chamber (7) can flow to the outlet (6) or down the diversion path to the

orifice plate (10). The amount of mass flow diverted is controlled by the pressure drop between diverter (7) and the drain cavity (12). As the orifice plate rotates, the volume of working fluid passing thorough changes resulting in a corresponding change in mass flow rate. When the disk is rotating, the diverted flow volume varies continuously creating fluctuations in the diverter chamber pressure. The magnitude of the pressure fluctuations or pulsation is controlled by the mass flow through the rotating orifice. The orifice throttle (8) controls the pulsation by obstructing the flow passage, artificially increasing the pressure drop between chambers (7) and (12). The pulsation can also be controlled by increasing the pressure in (12) and reducing the pressure drop across the orifice disk. As the pressure in the drain cavity (12) drops the water volume that seeps through the seals around the rotating shaft increases. The fluid that seeps through the seals is removed through a weep hole between the seal stack and the lower bearing casing. There are four pulsator inputs: the inlet pressure or mass flow, the orifice throttle position, the orifice disk rotation frequency, and the waste working fluid or back pressure valve.

2.4 Test Facility

The pulsator experiments were conducted in the UAHunstville Propulsion Center spray facility in the Johnson Research Center. The test facility provides the infrastructure including the hardware and software for conducting experiments. The test facility is split into two test areas, a high pressure spray chamber and an atmospheric test rig. Both test areas are controlled from a single command station. The atmospheric test rig was selected for the pulsator testing due to the accessibility

and flexibility that the facility provides. A 500 ft^3, high pressure air tank is located outside of the test facility and supplies gas simulant and pressurant to the facility. System pressurization is controlled with actuated valves and dome loaders controlled by low flow back pressure regulators. The pulsator motor is controlled through the command station through an inverter. Figure 2.2 is a diagram of the spray facility floor plan.

A schematic of the atmospheric test rig is shown in Figure 2.3. Working fluid flow is provided to the atmospheric test stand using a 60 gallon pressurized run tank. The run tank first filled from the Holding Tank containing filtered deionized water. The flow path between the holding tank and run tank is shut. The run tank is then pressurized by the high pressure air tank. The run tank pressure is controlled by setting the pressure with the back pressure regulator on the regulator panel and then opening the actuated valve. Working fluid is supplied to the atmospheric and high pressure spray rig via a 0.5 in seamless steel tubing.

The working fluid flow to the atmospheric test rig is controlled by two elements. The first element is a pneumatically actuated ball valve. The second is a variable area venturi to control the mass flow rate as a function of the up stream pressure and the venturi pintle position. The venturi is set by using calibration data for the two inputs. Due to the calibration's high uncertainty, the mass flow rate is measured using a timed capture of working fluid before running experiments. The pretest mass flow check provides a small well-defined mass flow uncertainty. As long as the tank remains pressurized at the same pressure, tests show less than 0.5% standard deviation in mass flow rate. The mass flow was measured each time the run tank

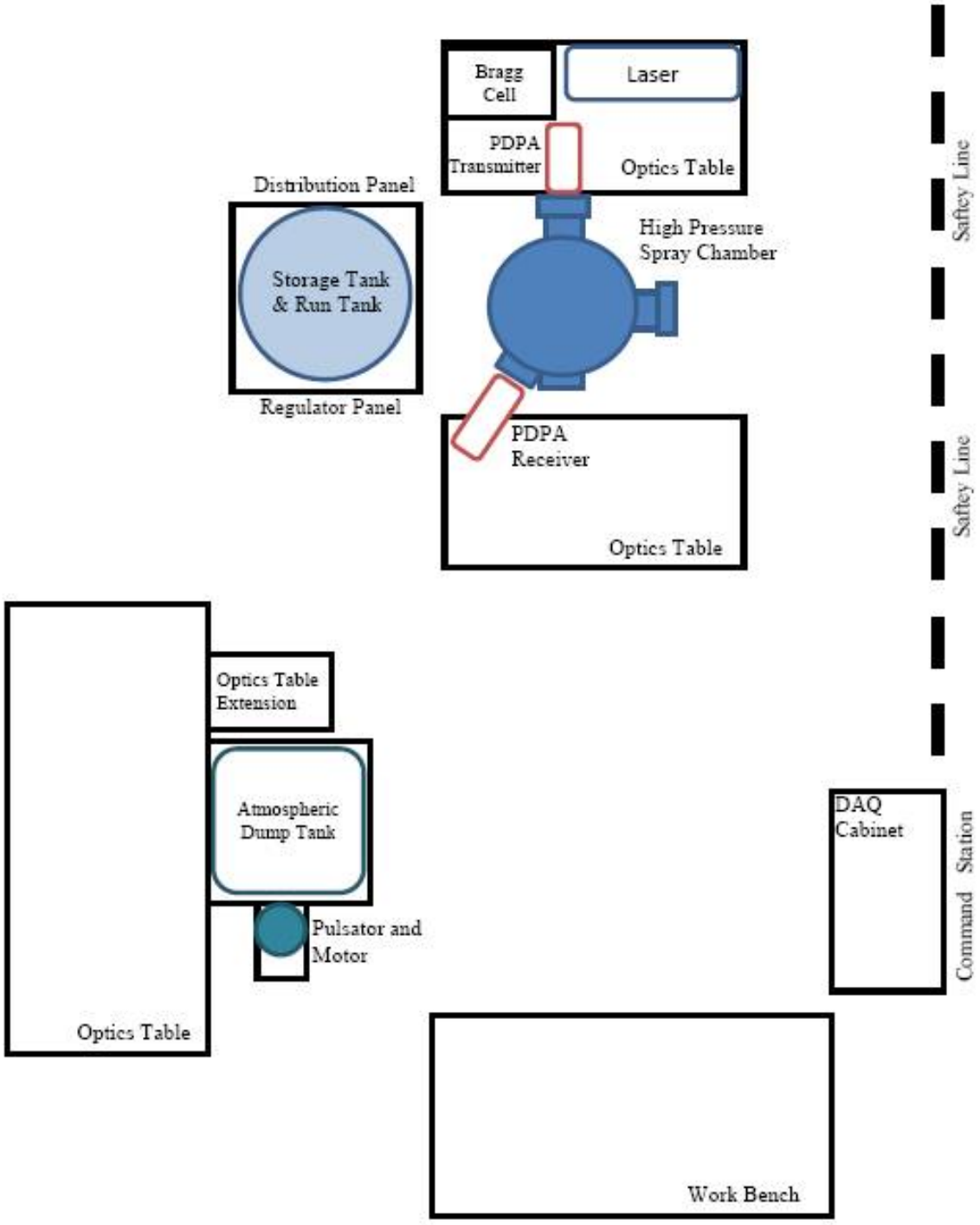

Figure 2.2: Floor plan of the PRC spray facility.

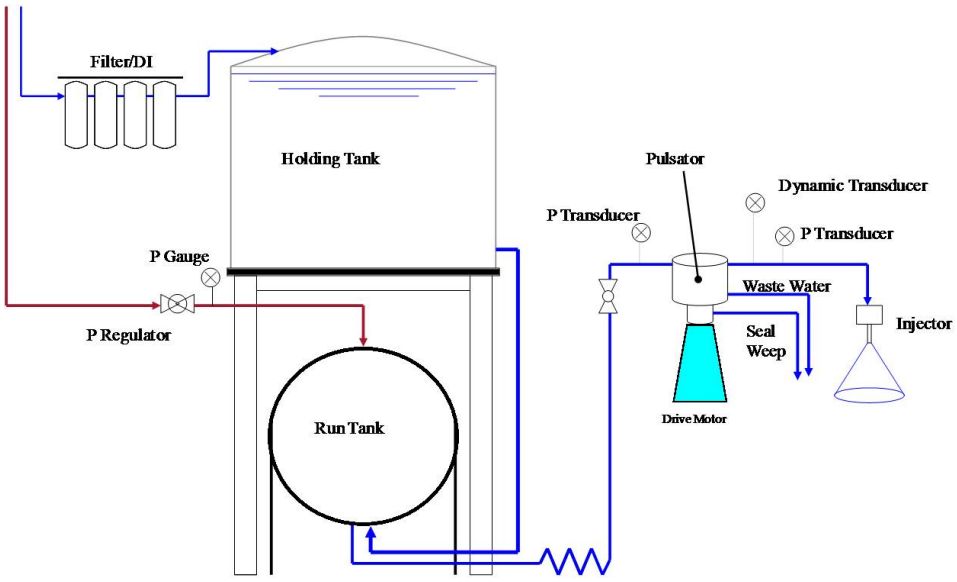

Figure 2.3: A side view representation of the PRC spray facility.

was depressurized or pintle position changed. From the venturi, ball valves direct the working fluid flow to the atmospheric or high pressure test facilities.

In the atmospheric spray rig, a manual ball valve can cut off flow as an additional safety precaution. Braided 0.5 in flexible steel tubing connects the pulsator input to the working fluid line and connects the pulsator output to the injector mounted in the test rig. The waste stimulant and seal weep are plumbed to flow into the dump tank beneath the injector.

2.4.1 Test Instrumentation and Data Acquisition

The facility uses pressure data and high speed imaging to examine the effects of the pulsator on the feed line pressure fluctuations. The high speed camera is a Phantom Miro 4 capable of recording 8,100 fps with a resolution of 256x256. Two different types of pressure transducers, static and dynamic transducers, were used. The static

pressure transducers are gage piezoresistive transducers with 9–28Vdc input, 0–5V output, and rated to 0.5% uncertainty at full scale output by the manufacturer. The transducers range from 0–750 to 0–5000 psi depending on the maximum pressure at the transducers' locations.

The transducers were recalibrated with the facilities including the power supply, data acquisition hardware and software. The uncertainty for the static transducers is calculated using Monte Carlo analysis. The pressure value has a 0.1% standard deviation. The standard deviation is taken using 6 voltage measurements at each data point. The average for each data point and the associated standards are used to generate a 10k set of data points using a normal distribution. The slope and intercept for each set of data points is calculated using a linear regression. The standard deviation is calculated for the slope and intercept. The uncertainty of the voltage measurement from the DAQ card resolution is $7.6 * 10^{-5}$. The resolution uncertainty is taken as a 95% certainty and half the uncertainty is used as the standard deviation. The resolution uncertainty is small enough that it is insignificant and not included in the uncertainty calculations. The calibrations produced on-site have an uncertainty of 0.1%, 0.16%, 0.14% and 2.1 psi for 750 psi, 1500 psi, and 3000 psi transducers, respectively.

The dynamic pressure is measured using a piezoelectric pressure transducer to obtain fast response times. When a piezoelectric material, such as quartz, is strained by an external force, it accumulates a charge on opposing surfaces. The transducer transforms the change in pressure to a force and the quartz crystal creates a high impedance voltage. The high impedance voltage is changed to a low impedance sig-

nal by a signal amplifier. The signal is then read by the data acquisition board. The precision required to do an on-site calibration is unavailable at the laboratory and the manufacturer's calibration is used as a result. The manufacturer's uncertainty is ±0.8%. Including the data acquisition card's resolution, the pressure uncertainty increases to ±(0.8% + .3) psi. The dynamic pressure transducer had a greater uncertainty than the static transducers. The desired pressure pulsations are over 15 psi, limiting the uncertainty to less than 3%.

The data acquisition and control has two aspects: the hardware and software. On the hardware side, the pressure transducers are wired to a connector panel to provide power and receive the signal output. From the panel, the transducers' signals are routed in to a BNC connector block rack. The block is connected into a NI PCI-6259 DAQ card. The data is collected from the DAQ card using Labview software. Labview is used to monitor the spray facility and to record data. Labview records data at 100kHz and produces a quick FFT to provide feedback on the operation and frequency of the pulsator.

2.5 Test Parameters and Matrix

The pulsator evaluation is broken down into five subsets: low pressure testing, high pressure pulsation verification, repeatability, position testing, and detailed testing. The initial low pressure characterization was limited in scope because of system limitations when testing first started. When high pressure capabilities came on-line, initial testing demonstrated the necessity to start with low expectations of the pulsator and work up to a full characterization. The second set is the first high pressure

experiments and focused on establishing the presence of pressure pulsations and the pulsation frequency. The third set examines the repeatability of the pulsation amplitude generated by the pulsator. The fourth test set focused on determining the pulsation throughout the feed system. The fifth looks at characterizing the pulsation behavior to set pulsation frequency, mass flow output, pressure output, and pulsation magnitude for injector testing.

2.5.1 Low Pressure Testing

The low pressure tests were performed to obtain a full characterization of the pulsator's response. The number of controls and time limited the spectrum of the tests to a generalized characterization and technological demonstration. The tests were conducted changing the four input variables: driving pressure, motor and pulsator frequency, orifice throttle, and back pressure throttle. The pressure set points were controlled by the pressurization capabilities at the time the tests were preformed. The second variable, frequency, values were chosen to match the CFD preliminary design analysis done on the basic pulsator geometry. For the throttle variables, an initial round of testing was performed over the entire valve ranges measured in percent open. The investigation determined the range over which the effect on output variables was significant. The values for testing the throttle controls were then chosen accordingly. Zero was not chosen as a set point for either throttle because the pulsator requires some fluid flow to function as lubricant and coolant. The set points for the variables are listed in Table 2.2.

Table 2.2: Low Pressure Characterization Set Points

Control Variable	Units	Set Points
Pre Pulsator Driving Pressure	psig	160, 200
Motor & Pulsator Frequency	Hz & Hz	75, 90 & 1575, 1890
Orifice Throttle	% Open	6.8, 13.6, 27.2, 40.9
Back Pressure Throttle	% Open	5.6, 11.1, 22.2, 33.3

The low pressure test's experimental set-up was different from the high tests due to the facility limitations when the tests were conducted. The system was pressurized by a K bottle instead of the main tank. The K bottle limitations guided the pressure set points. Additionally the data was taken at a lower frequency, 30 kHz versus the 100 kHz the high pressure data was taken at. The pressurization and data capture rate were the only significant changes to the experimental method.

The tests were conducted by first filling the stimulant run tank. The run tank was pressurized by setting the desired pressure on the pressure regulator. As the pressure regulator was opened, the run tank was pressurized because the K bottle did not have an actuated valve in-line to the run tank. After the run tank was pressurized, the throttles on the pulsator were set for the specific test set point. At that point the flow would then be initiated and the pulsator started. After ten seconds, the test data recording would start. Using two collection devices, a timed capture of mass from the waste lines and injector was measured. Data recording was stopped after ten seconds. When the mass collection was finished, the pulsator was shut down, then simulant flow was stopped using the actuated valve. At this point, the run tank

could be refilled, the system pressure reset, or the testing could continue at a new set point. This process was repeated until all of the test points were covered.

2.5.2 High Pressure Pulsation Verification

The first set of high pressure tests determines if the pulsator functions and if the frequency of pressure waves in the output match the frequency the pulsator is set to generate. The two primary sources of data for the pulsation test were the dynamic pressure transducer data and the high speed video. The tests were chosen to see if the pulsator performed at the maximum pulsation frequency and at the highest diverted mass flow fraction. The pulsation testing frequency is 2100 Hz. The highest diverted mass flow fraction is assumed to produce the highest pulsation magnitude; therefore, the throttle orifice was set to 100%, 3.67 turns, open, and the back pressure orifice is set to 100%, 9 turns, open. Based on the pulsator design, 67% of the working fluid is expected to be diverted to the waste lines. In order to match the nominal flow rate for the first injector, the pulsator will be tested with, the non-diverted mass flow rate needs to be 0.18 lb/s. Thus, the venturi was set to have a mass flow of 0.56 lb/s. The mass flow rate was first confirmed by diverting the working fluid to a spigot and using a timed flow capture to confirm the mass flow rate. If the mass flow rate was off by more than 5%, the venturi pintle position was adjusted and the flow is retested. When the error in mass flow rate was less than 5%, the mass flow rate was measured a second time to confirm the mass flow rate. During the tests, video was taken of the flow and one second of data was recorded after a period greater than ten seconds after the pulsator was started. The mean mass flow rate was also used

Table 2.3: Repeatability Test Summary

Test Name	Number of Set Points	Number of Tests
On/Off Repeatability	1	8
Throttle Repeatability	2	4

Table 2.4: Repeatability Test Set Points

Set point	Mass Flow Rate	Frequency	Orifice Throttle	Back Pressure Throttle
Units	lb/s	Hz	% Open	% Open
On/Off	0.56	2100	22	18
A	0.56	2100	9.1	5.6
B	0.56	1575	100	100

to generate a non-pulsed flow video to compare to the pulsed video. After collecting high speed images with the pulsator frequency set to 2100 Hz, the flow route was plumbed around the pulsator and the venturi mass flow rate was reduced to match the injector flow rate measured during the pulsed test. Tests could then be performed at other frequencies to see if there are increases in visual pulsation in the high speed video.

2.5.3 Repeatability Testing

Repeatability testing was used to determine if the pulsator's pressure oscillations are repeatable and if any differences can be quantified. The tests are separated into two parts on/off and throttle repeatability listed in Table 2.3. On/off repeata-

bility tests use a single test point that the flow and pulsator are turned off and on between tests. The on/off test point was performed under the same conditions as the pulsation presence tests, Table 2.4: 2100 Hz pulsation, orifice throttle position of 100% open, back pressure throttle position of 100% open, and a mass flow rate of 0.56 lb/s. Similar to the pulsation tests, the mass flow rate is first checked using the time capture method before starting testing. If the run tank is depressurized, the mass flow rate is verified before continuing testing. After the mass flow rate is correctly set, the throttles are set. Then, the scale is zeroed with the mass collection container. Simulant flow is then started and the pulsator is started. Mass flow capture begins ten seconds after the pulsator is started, but only the injector mass flow is captured during the on/off repeatability tests. After the mass flow capture starts, data is recorded for one second at 100 kHz. When the mass flow capture is finished, the pulsator and simulant flow are stopped and repeated until all eight test have been performed.

The second part of the repeatability testing is the throttle repeatability. The throttle repeatability is focused on determining if the uncertainty of the throttle position introduces significant variation in the pulsation. The test uses two set points identified as A and B. Each set point has the same flow rate through the injector, but different settings for the pulsator orifice throttle, back pressure throttle, and pulsator frequency. The tests are conducted by running the first point, then stopping the tests, resetting controls for the second test point, and testing the second test point. The alternating pattern continues until four tests are completed for each test point. Similar to the previous test, the mass flow is confirmed before starting testing, but not

in between unless the run tank has been vented. During the test, the mass flow rates are measured for the waste, weep hole,and injector. The mass flows are measured by using three discrete containers to capture the flow at each source sequentially. The mass of each container was measured before and after each test.

The specifics of the two test points are listed in Table 2.4. The throttle values used for each of the set points are at opposite ends of the spectrum, to determine if there is variation between the ends of the control ranges. The low throttle values were also selected to coincide with the lower frequency because the slower rotating disk allows more simulant to pass through the disk as waste. Set point A uses closed throttles to generate low pulsation. By choosing a low and high pulsations settings, the test will show if pulsation magnitude has an effect on the repeatability. Set point B uses open throttles to generate large pulsations. The A and B set points should test the extremes of the pulsation range. In contrast, the frequency values do not cover the entire pulsator range because the expected primary testing range with the pulsator is between 1500 to 2100 Hz. The low end of the frequency range is not covered.

2.5.4 Position Testing

The next set of experiments, position testing, focused on evaluating the influence of the pulsator on other parts of the feed system. More specifically, the experiments were performed to determine if the pulsation generated at the pulsator travels upstream as well as downstream, and how the pulsation amplitude changes as the pulsation moves away from the pulsator. The other test performed only uses a

dynamic pressure transducer at the pulsator outlet. To examine the pulsation impact throughout the system, independent tests were conducted with the dynamic pressure transducer at five different locations throughout the system: immediately before the injector, the pulsator outlet, the pulsator inlet, immediately downstream of the flow control venturi and immediately after the run tank. The injector is approximately 26 inches downstream of the pulsator, and the venturi is approximately 25 feet upstream of the pulsator. Moving the same transducer to different locations could cause because sections are depressurized and drained could cause inconsistencies between the data sets. The system is comprised of 0.5 inch tubing. The dynamic transducer is mounted into a tee, and the tee is moved to various locations. The tests are performed moving from the injector towards the run tank. The three positions in the atmospheric spray rig are performed without depressurizing the system. The venturi and run tank positions require the depressurization and draining of tubing. The draining of tubing and depressurization require the mass flow rate to be rechecked. The depressurization and pressurization increases the uncertainty in the correlation between the tests.

The general high pressure characterization is similar to the low pressure characterization. Testing constraints make the testing matrix similar in size to the low pressure test matrix. Table 2.5 has the test matrix of the high pressure test data and the low pressure test matrix is in Table 2.2. The frequency test points are set to outline the primary test range. The preliminary tests were used to determined the throttle positions for the set points. Using an oscilloscope, the valves were independently analysed to find the inflection points of the graphs. Under the assumption

Table 2.5: High Pressure Characterization Set Points

Control Variable	Units	Set Points
Run Tank Pressure	psig	706
Mass Flow Rate	lb/s	0.56
Motor Rotational Frequency	Hz & Hz	75, 100 & 1575, 2100
Orifice Throttle 1575Hz	% Open	8.9, 13.6, 100
Orifice Throttle 2100Hz	% Open	15.8, 22.6, 100
Back Pressure Throttle	% Open	5.5, 11.1, 22.2, 33.3, 100

that zero is the first inflection point and unusable as a test point, the first inflection point is a maximum. The first inflection test was conducted to find the orifice throttle positions with a mass flow rate of 0.56 lb/s and the back pressure throttle was set to 100% open. For each frequency value, three points were found: a maximum, a minimum, and a slow increase to the maximum throttle position. The same was done for the back pressure throttle. For each throttle position, the back pressure was scanned to determine the inflection points in the pulsation magnitude. After scanning three different orifice throttle positions, the significance of the change in pulsation magnitude could not be determined on the oscilloscope. As a result five back pressure data points were chosen instead of the inflection points. The back pressure set points are the same as the low pressure set points with the addition of the maximum throttle position.

2.5.5 General Characterization

All of the test conditions were performed with the same mass flow rate 0.56 lb/s, resulting in the total test matrix, shown in Table 2.5, for a total of 30 tests. The mass flow for each of the outflows varied for each test point. The tests were conducted in the same method as in the previous test. The system is checked, initialized, and the run tank filled. The run tank is filled from the holding tank. The venturi is set and checked for the desired mass flow rate. The throttles are set, flow is started, the pulsator is started, and the mass and data collection started. The mass flow rate for each of the three outputs were measured using the same technique as the previous test sets. The data is collected during the test and the real time data is monitored from the control station but is not analysed or processed in real time due to the volume of data collected.

2.6 Data Processing

The data processing is separated into two parts. The first part is running the data through a Matlab program to obtain a spectrum analysis of the feed line pressure signal and the average peak to peak pressure difference. The voltage data is converted to pressure using the calibration data. The spectrum analysis is accomplished using a predefined Matlab function. The Matlab program outputs the spectrum analysis in the form of a signal magnitude in the frequency domain and a 0.01 second pressure waveform graph. Figure 2.4 is an example of the output from the Matlab program. The other primary function of the Matlab program was to determine the peak to peak

pressure pulsation amplitude. The pulsator was expected to produce a non-sinusoidal signal. As a result the amplitude information from the FFT was not be particularly helpful to determine the peak to peak amplitude. To get a better peak to peak amplitude, the Matlab program uses a custom algorithm to determine the amplitude. The algorithm first finds the frequency corresponding to the highest magnitude wave from the FFT data above 50 Hz. The number of data points to cover one cycle is calculated. The number of data points is increased to cover 1.25 cycles to guarantee at least one maximum and minimum in each set of data points. Within the 1.25 cycles of the dominant frequency, the maximum and minimum are found. The average difference between the maximum and the minimum and the data points before and after them are found. The use of three data points minimizes the impact of an outlier. The algorithm moves on to the next set of data points and averages with the result from the first data set. The entire data set is processed to obtain the average peak to peak amplitude. The Matlab code also finds the average and standard deviation for each of the values recorded by Labview.

The second part of the data processing was a subjective comparison of different variables. The data from individual tests were graphed against each other to determine if there were patterns in the results. In addition to finding patterns, the graphing analysis provided a guide to develop a methodology to iteratively tune the pulsator to a specific set point. These set points were for injector testing and included the pulsator outputs such as feed line pressure and mass flow rate. The graphing was done using Microsoft Excel to quickly change the graphed variables to maximize the information extracted from the raw test data.

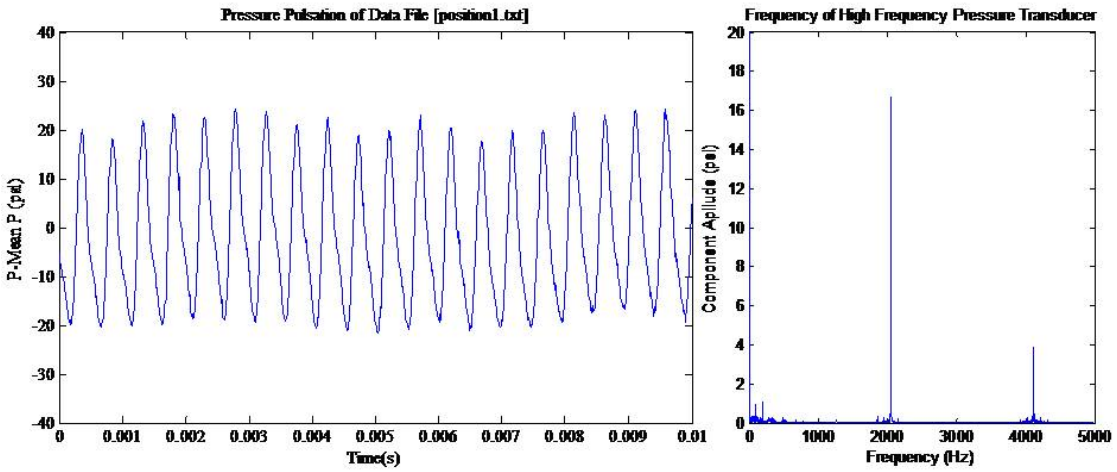

Figure 2.4: An example of Matlab code output.

2.7 Uncertainty and Assumption Summary

The uncertainties and assumptions are an important part in defining the application as well as the experiment results. The uncertainties and assumptions place limitations on the static pressure sensors, mass flow measurements, pulsator tuning, and the data processing. The static pressure measurements have an uncertainty of less than 2.2 psi. It is assumed that the noise caused by the three phase motor does not increase the uncertainty of pressure measurements. The three phase motor generates 180 Hz noise, which increases the standard deviation of the data, but because 100k samples are average for each value, it assumes the the noise is accounted for in the average. The venturi mass flow rate has an uncertainty below 0.01 lb/s. During early testing, poor procedures resulted in mass flow outliers. Since new procedures were developed, no outliers have shown up and the chance of outliers is assumed to be negligible. The uncertainty for the mass flow rates measured at the outlet have an

uncertainty of 0.0035 lb/s dominated by the time measurement. The throttles have resolutions of one sixth and one half turns, but have uncertainties of a sixteenth and eighteenth of a turn respectively. The peak to peak pulsation amplitude is defined as the average difference between the maximum and minimum for each cycle. The FFT analysis has a one-hertz resolution. The uncertainties and assumptions are important factors limiting the experimental results.

CHAPTER 3

EXPERIMENTAL RESULTS

I have yet to see any problem, however complicated, which, when you looked at it the right way, did not become still more complicated.

—Paul Alderson

3.1 Pulsation

The first set of experiments focuses on establishing the pulsator functionality to produce substantial pulsation in the high frequency combustion instability frequency range. The evaluation was performed by examining the response from both high speed video and the dynamic pressure transducer data at 100 kHz. Figure 3.1 is a comparison between the dynamic pressure transducer response when the pulsator is off and when it is on. When the pulsator is turned off, the signal is consistent with system noise and does not have any frequencies in the FFT with magnitudes over 0.25 psi. When the pulsator is on, clear pressure fluctuation can be seen in both the waveform and the FFT results. The FFT reports a dominant frequency, 2098 Hz, less than 0.1% off from desired output, 2100 Hz. The frequency output from the pulsator is the pulsator input ± 4 Hz.

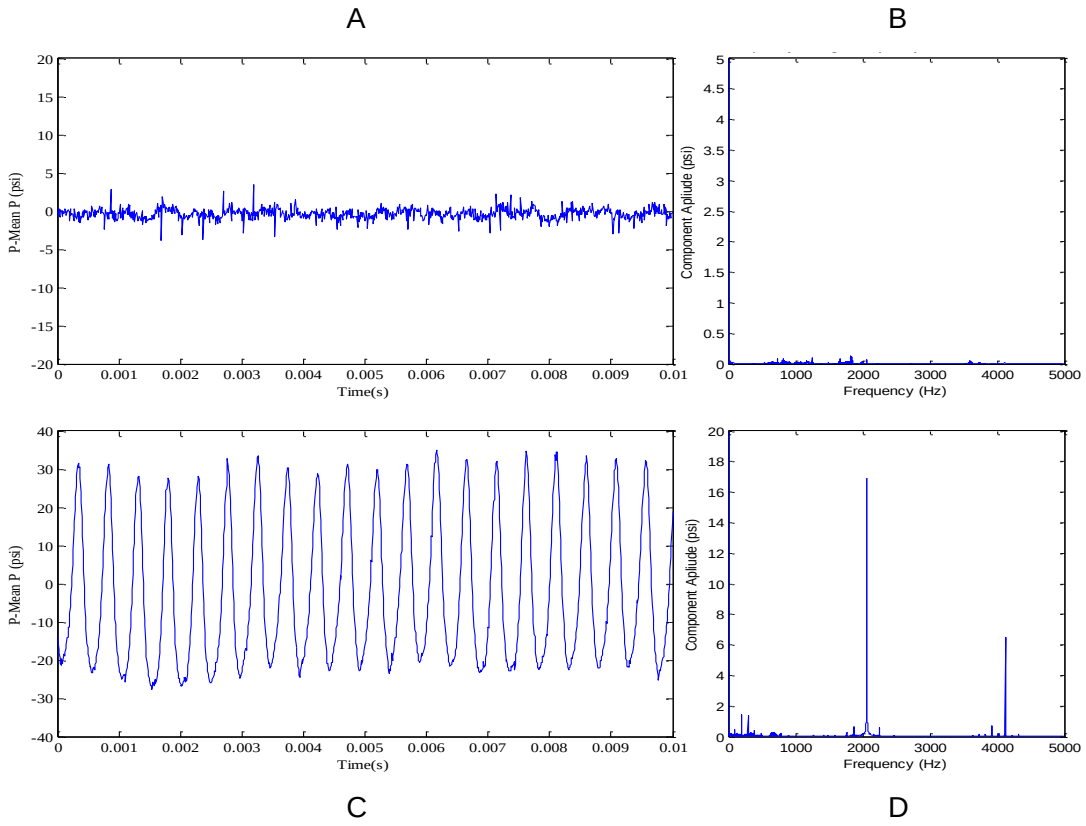

Figure 3.1: Comparison of dynamic transducer data with the pulsator On and Off. A) Waveform with pulsation B) FFT with pulsation C)Waveform without pulsation D) FFT without pulsation

The FFT produces the frequencies and magnitudes of sine waves making up the pressure waveform. The first harmonics amplitude is 17 psi. The second harmonics amplitude is visible in Figure 3.1 D. The second harmonic is significant because the pressure pulsations have a non-sinusoidal shape. The dominate frequency amplitude is 17 psi resulting in a peak to peak magnitude of 34 psi. The dominate frequency peak to peak magnitude represents the waveform peak to peak pulsation poorly. The waveform shows that the pressure varies from -20 to 30 psi clearly larger than the 34 psi FFT result. In contrast, the peak to peak algorithm produces 54.5 psi. The

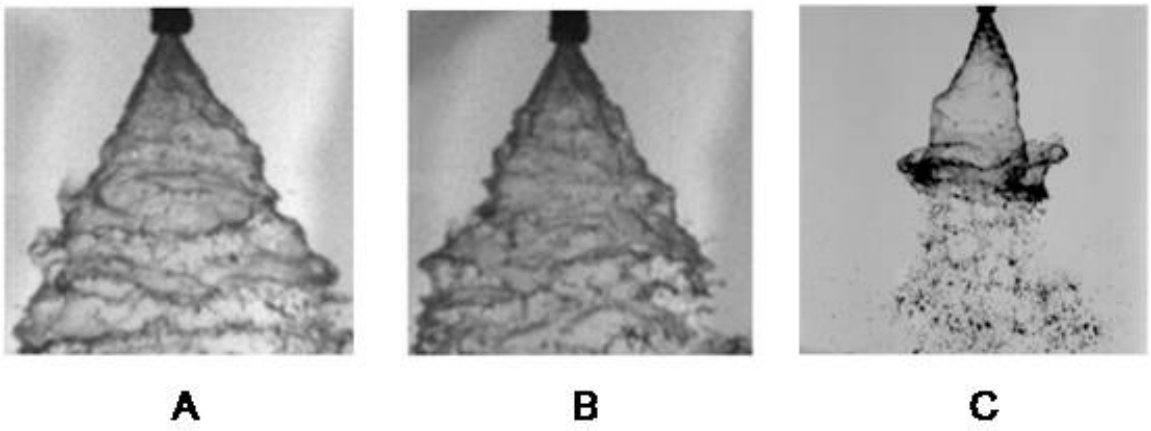

Figure 3.2: Images from the high speed video A)2100 Hz Pulsed Flow B) No Pulsation C) 105 Hz Pulsed Flow.

algorithm produces a better estimate of waveform pulsation magnitude evaluation using the harmonics magnitudes from the FFT results.

Pressure fluctuations are expected to be visible in high speed video capturing the injector spray. Video is captured from the injector during steady and pulsed conditions. The steady flow video is taken matching the injector mean mass flow rate during the pulsed flow video. The video is taken at 128x128 and 25 kfps resulting in 11.9 frames per pulsation cycle. Figure 3.2 A and B show typical images captured from the high speed video for both the pulsed and steady flow. The images and video show no apparent differences between pulsed and steady flow. Performing some detailed image analysis on the video may show pulsation effects that are not apparent to the eye. The high frequency pulsations may not be noticeable in the image partially because the induced fluctuations have roughly the same time constant as the natural waves. Earlier data showed that the pulsation magnitude increased when the frequency was reduced. Therefore, the video was taken at lower frequencies in an

attempt to produce clear visual evidence of the pulsator function. 105 Hz, 210 Hz and 420 Hz pulsation frequencies were tested and filmed using a high speed video recorder at 8100 fps. Figure 3.2 C shows an image captured from the 105 Hz frequency test. The video showed dramatic changes in spray angle and flow velocity clear evidence of pulsator operation. The high pressure resulted in higher mass flow and a decrease in spray angle creating a wave in the spray sheet. Figure 3.2 C shows the high velocity section passing the slower spray sections and triggering sudden increases in the sheet break up. The low frequency pulsation video indicated that the differences between the original 2100 Hz and non pulsed flow video are not necessarily caused by a lack of pulsation. The similarities between the 2100 Hz tests were caused by a weak pulsation magnitude, and more specifically the pulsation magnitude compared to the pressure drop across the injector. When a rocket engine has 10% pulsation and a 500 psi chamber pressure, the pressure pulsation is 50 psi. An injector in this particular rocket engine only has a pressure drop of 40 to 70 psi across the injector. The 50 psi pulsation causes pressure variations ranging from 70% to 125% pressure drop across the injector. In the atmospheric spray facility, the pulsation percentage is equal to the percent pulsation drop across the injector. Specifically the 2100 Hz data in Figure 3.2, the 50 psi pulsation is 21% pulsation, but it is also only has a 21% pressure drop across the injector. When the frequency was increased from 105 Hz to 210 Hz and 420 Hz, the pulsation in the video decreased. At frequencies higher than 420 Hz, observable pulses in the spray were no longer visible. Although the pulsation effects were not visible in the 2100 Hz pulsation, the dynamic pressure transducer

data and the lower frequency video show the presence of pulsation in the pulsator output.

3.2 Repeatability

Repeatability testing was conducted in two parts. The first part involved operating at fixed system flow control and pulsation settings. The first test set was to establish the repeatability of turning simulant flow and the pulsator on and off. The on/off repeatability testing process was repeated eight times. While there were similarities in the test data, the dominant frequencies' amplitudes were substantially different. Table 3.1 summarizes the eight tests results. The table gives the average dominant frequency and the second harmonic pulsation magnitude. The values determined using the peak to peak algorithm are given under the row title "Pulsation." The values from the FFT are given under the rows "1st Harmonic" and "2nd Harmonic." The ratios between second and first harmonic magnitudes are also given in the table. The initial analysis yielded large standard deviations, on the order of 60% for the dominant frequency. A single outlier was removed from the data set; the average and standard deviation were calculated again. Removing the outlier resulted in a significant reduction in the standard deviation. The pulsation magnitude from the peak to peak analysis was reduced from 60% to 17%, while the FFT first harmonic magnitude is reduced from 66% to 36%. The pulsation variation is a cause for concern as the testing represented the most basic form of pulsator repeatability testing. No rational could be developed for the large standard deviation seen in this testing. From examining the waveform, the problem appears to be with the second harmonic

Table 3.1: On/Off Repeatability Results Summary

	Avg	σ	$\frac{\sigma}{Avg}$
Pulsation	20.5	12.2	60%
1^{st} Harmonic	9.2	6.1	66%
2^{st} Harmonic	3.4	1.4	41%
2^{st}:1^{st} ratio	2.6	0.7	27%
Remove Outlier			
Pulsation	20.6	3.6	17%
1^{st} Harmonic	7.4	2.7	36%
2^{st} Harmonic	2.0	0.4	20%
2^{st}:1^{st} ratio	3.7	0.7	19%

magnitude and phase shift, but the source is unknown. The variation in replicating the pulsation is problematic for testing, but the pulsation tests show the capability to generate pulsations over 50 psi and over 10%. The pressure pulsation standard deviation and the mean provide that 79% of the time the pulsator will generate more than 10% pulsation. As test points are found that produce greater pulsation, it is expected that the 10% pulsation rate will rise significantly.

The second set of repeatability testing used two test points identified as A and B. Each set point had the same total mass flow rate flow rate, but different settings for the pulsator orifice throttle, back pressure throttle, and pulsator frequency. The data for the first point, A, Table 3.2, exhibited similar results as the data from the on/off repeatability testing. The peak to peak pulsation standard deviation was 54%. The first and second harmonic amplitude standard deviations were 47.3% and 46.2% respectively. The large standard deviations suggest that there is very little control

Table 3.2: 2100 Hz Throttle Repeatability Set Point Summary

	Avg	σ	$\frac{\sigma}{Avg}$
Input P (psi)	459	42.8	9.3%
Waste P (psi)	331	39.4	11.9%
Injector $\dot{m}$ (lb/s)	0.231	0.01	14.3%
Waste $\dot{m}$ (lb/s)	0.113	0.02	17.2%
Dump $\dot{m}$ (lb/s)	0.192	0.04	20.8%
Pulsation (psi)	67.7	32.7	46.8%
Pulsation (%)	15.0	7.0%	46.8%
1^{st} Harmonic	33	15.6	47.3%
2^{st} Harmonic	3.25	1.5	46.2%
2^{st}:1^{st} ratio	0.11	0.06	54.5%

over the pulsation magnitude. There is one data point that can be classified as an outlier, but due to the number of data points, it cannot be removed using Chauvemet's rejection criteria. By removing the data point anyway, the data improves dramatically. Table 3.3 shows the recalculated results after removing the data point. Similar to the on/off repeatability testing, the peak to peak standard deviation and the first harmonic amplitude is reduced to 21.5% and 24.9% respectively. The second harmonic standard deviation did not change substantially. The data indicate variability in the pulsation magnitude and larger variations in the waveform shape. The pulsation only has a standard deviation of 22%, but the second harmonic has a 44.4% variation. The second harmonic amplitude is phase shift dependent and whether the second harmonic produced constructive or destructive interference with the waveform's peaks. The data indicates that the poor repeatability in this instance may not be due to the uncertainty in resetting the control variables, but may be

Table 3.3: Corrected 2100 Hz Throttle Repeatability Set Point Summary

	Avg	σ	$\frac{\sigma}{Avg}$
Input P (psi)	438.2	6.7	1.5%
Waste P (psi)	312	12.5	4.0%
Injector $\dot{m}$ (lb/s)	0.23	0.01	4.3%
Waste $\dot{m}$ (lb/s)	0.12	0.01	8.3%
Dump $\dot{m}$ (lb/s)	0.18	0.04	22.2%
Pulsation (psi)	54.0	11.6	21.5%
Pulsation (psi)	12.3	2.6	21.4%
1^{st} Harmonic	25.7	6.4	24.9%
2^{st} Harmonic	2.7	1.2	44.4%
2^{st}:1^{st} ratio	0.11	0.07	63.6%

due to some additional unknown phenomena in the system causing the change in the waveform shape.

Table 3.4 gives the set point B repeatability test results. The B set point produced no outliers unlike both tests at 2100 Hz. The data show the same results; a high standard deviation for the pulastion data and low standard deviations for the static measurements. The mean mass flow consistency and pressure values indicate that the variation in the data has to do with the pulsation mechanics and not the system as a whole. The results from all of the data sets show that the mean values are significantly more reliable than the varying values. The static test conditions are reproducible.

The test results from A and B are both irregular. If injector testing is dependent on producing pressure pulsation greater than a certain threshold, the performance becomes better. Table 3.5 lists the pulsation thresholds and the chance that

Table 3.4: 1575 Hz Throttle Repeatability Set Point Summary

	Avg	σ	$\frac{\sigma}{Avg}$
Input P (psi)	171	4.4	2.6%
Waste P (psi)	17.4	0.4	2.3%
Injector $\dot{m}$ (lb/s)	0.14	0.002	1.4%
Waste $\dot{m}$ (lb/s)	0.399	0.01	2.5%
Dump $\dot{m}$ (lb/s)	0.01	0	0.0%
Pulsation (psi)	64.7	20	30.9%
Pulsation (psi)	37.7	11.6	30.9%
1^{st} Harmonic	27.5	9.3	33.8%
2^{st} Harmonic	4.75	1.3	27.4%
2^{st}:1^{st} ratio	0.2	0.12	60.0%

Table 3.5: Pulsation Threshold Table

Threshold	2100 Hz	2100 Hz Modified	1575 Hz
P' > 10%	76.1%	80.8%	99.1%
P' > 20%	—	—	93.6%
P' > 30%	—	—	75.5%

the pulsator will generate pulsation above the particular thresholds. The pulsation at the B test position produces large pulsations and has a 90%+ chance that the pulsator will generate pulsations over 20%. In contrast, the A test data is taken at low throttle positions and should generate pulsations significantly below the maximum pulsation capabilities at 2100 Hz. The mean pulsation percentage doubles between tests A and B. The increase in the pulsation magnitude comes from both the feed

line pressure and pulsation magnitude. The pulsation magnitude increases 20% and the mean feedline pressure drops 60%.

3.3 Pulsation in System

The next experiment set focuses on evaluating the pulsators influence on other feed system parts. More specifically, the experiments set out to determine if the pulsation generated at the pulsator travels upstream as well as downstream, and how the pulsation amplitude diminishes as the pulsation moves away from the pulsator. To look at the effects of pulsation throughout the system, independent tests were conducted with the dynamic pressure transducer at five different locations throughout the system. The first point, immediately before the injector, is 1 inch from the tangential inlets to the swirl injector. The pulsator outlet location is 3 inches from the rotating disk and 28 inches from the injector. The pulsator inlet measurement is taken 2 inches from the rotating disk. The downstream venturi location is 25 feet upstream of the pulsator and 6 inches downstream of the venturi. The last location is in between the run tank and the venturi. The pulsation amplitude at each point is shown in Figure 3.3. Two lines outline the upper and lower pulsation range limits. The tests' repeatability should be taken into account when looking at the results. For each test point, only two tests were performed. If one of the data points is an outlier, the results would be thrown off significantly. In this testing there is no way to determine if an outlier is present without taking more data.

As expected, the largest amplitude occurred immediately upstream of the pulsator and the amplitude decreased as the transducer is moved further away from

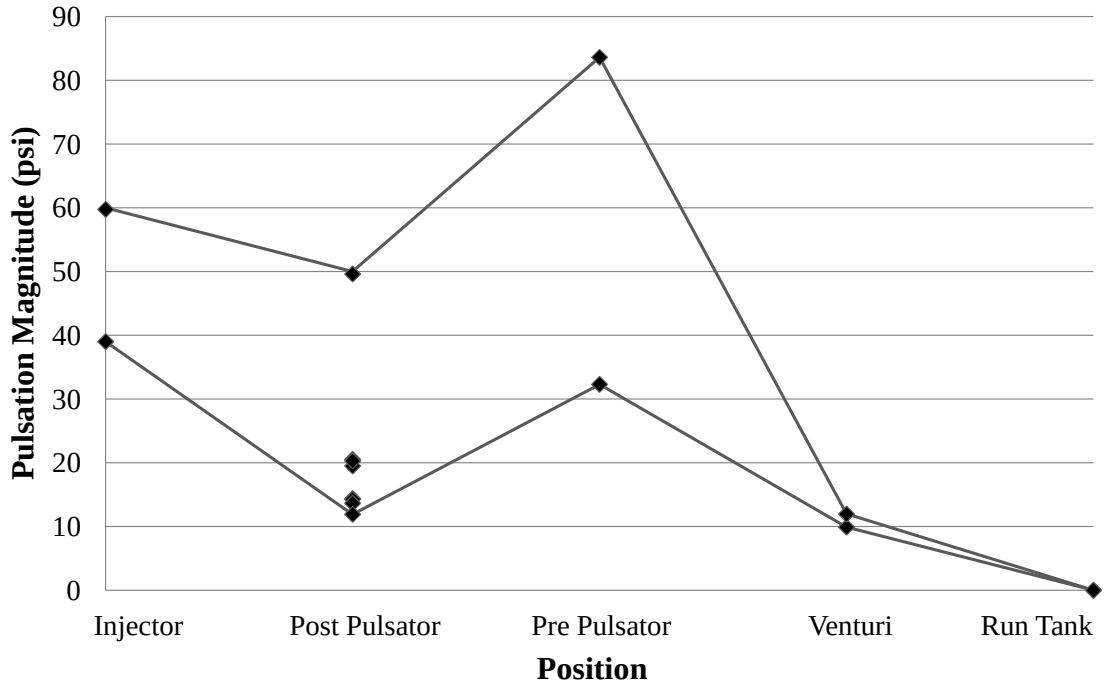

Figure 3.3: The pulsation magnitude is graphed against position. The x axis is not representative of the distance from the pulsator.

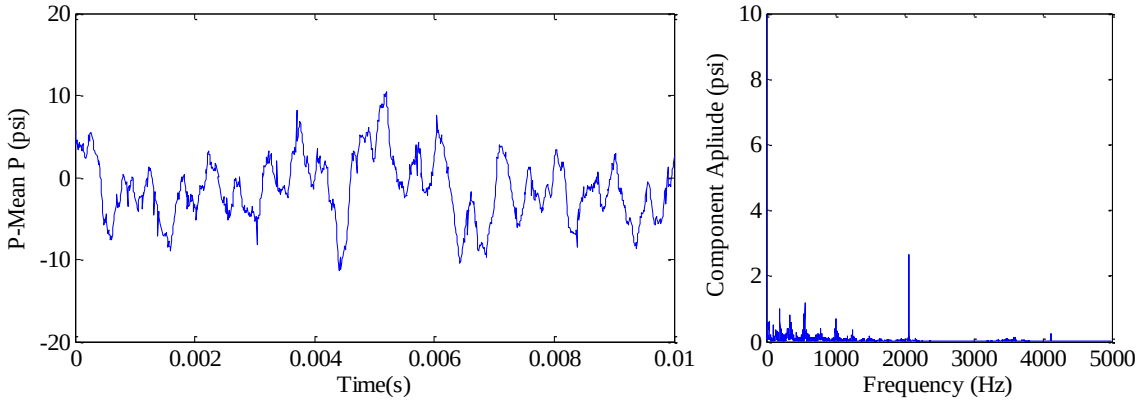

Figure 3.4: The graph includes a waveform section and the FFT frequency results down stream of the venturi.

the pulsator. As the pulsation magnitude drops, the data becames more consistent. At the venturi and the run tank, the values are almost identical. The run tank pressure results are in line with expectations; there are no pressure fluctuations in the dynamic pressure transducer data, and the data has a similar appearance to the no pulsation data taken during the pulsation presence tests. The venturi waveform, Figure 3.4, has a 10 psi average peak to peak pressure oscillation and has large amounts of noise present in the signal. The venturi waveform FFT shows several frequencies above 0.5 psi. The FFT with the pulsator off shows no peaks above 0.5 psi. The peaks in the venturi data may originate from the pulsator or from cavitation through venturi. The pre pulsator data has significantly less noise than the venturi data. It also has the largest pulsation magnitude and is closest to the orifice disk. The post pulsator pulsation magnitude is significantly lower than the magnitude on either side. Because the pulsation increases downsteam of the post pulsator data, the data is considered to be an outlier. The higher pressure pulsation magnitude could be caused by a standing wave from the high impedance of the injector inlets. A standing wave is ruled out because over lapping data from the other test produce higher pulsation magnitude. Further testing is necessary to completely rule out a standing wave. The data used was taken as a part of the on/off repeatability study and provides eight data point, rather than the two data points all the other location tests had. The dip in pulsation could be inconsistent data, or resulting from the test taking place on different days and changing an unknown system variable.

3.4 Low Pressure Characterization

The initial pulsator characterization was limited in scope because the number of control variables, time, and early facilities limitations. The pulsator requires four variables to be controlled for a complete characterization. The technological demonstrations and characterization tests were conducted at a constant initial flow rate. The pulsator input pressure was set with the pulsator off and the waste water valve shut. The pressure was left unadjusted for a series of tests. This is contrary to most injector designs where tests are performed with selected mass flow rates. Since a characterization was being performed, the pressure was selected, the mass flow rate was treated as an output variable and measuered at each set point. The pulsator pressure and the injector pressure were measured with each test. As the pulsator settings were changed, the mass flow rate through the waste water line and seal weep changed. The desired pulsation frequency was controlled by changing the rotational velocity of the orifice disk and the motor attached to it. The frequency response was captured by the dynamic pressure transducer. The throttle values serve as the primary pulsator controls. The physical characteristics of the knobs were used as units to measure the valves positions. Each of the four control variables was examined to determine the influence over the pulsator output. Each variable's magnitude, influence and the range over which it is significant was evaluated.

3.4.1 Initial Pressure Control

The pressure setting is one form of control and is not expected to be changed during an injector test to fine tune the pulsator's output. The low pressure testing uses only two pressure values because the compressed gas volume in a K-bottle is relativity small. The amount of waste working fluid the pulsator consumes requires a large amount of compressed air to pressurize and drive the working fluid. Even during the current tests, a single K-bottle only provides pressurization for 15 tests. To run a set of tests at a higher pressure requires more than one K-bottle for a single 60 gal run tank. In addition to requiring more pressurized gas to drive the run tank, the increased pressure increases the amount of water the pulsator and injector consume because of the increased mass flow rate. The initial pressure change would provide greater control over the desired mass flow rate. The increase in pressure generates a larger mass flow rate and increases the maximum pulsation.

3.4.2 Frequency Control

The frequency control was a major part of testing. An important factor was confirming the fluid response to the pulsator input. The frequency was increased from 1575 Hz to 1995 Hz. The change in frequency represents a 27% increase in frequency with only a 5% decrease in injector pressure. The two frequency values were chosen based on an earlier CFD design study that was performed while the pulsator was in the design process. The preliminary testing showed that the frequency would not

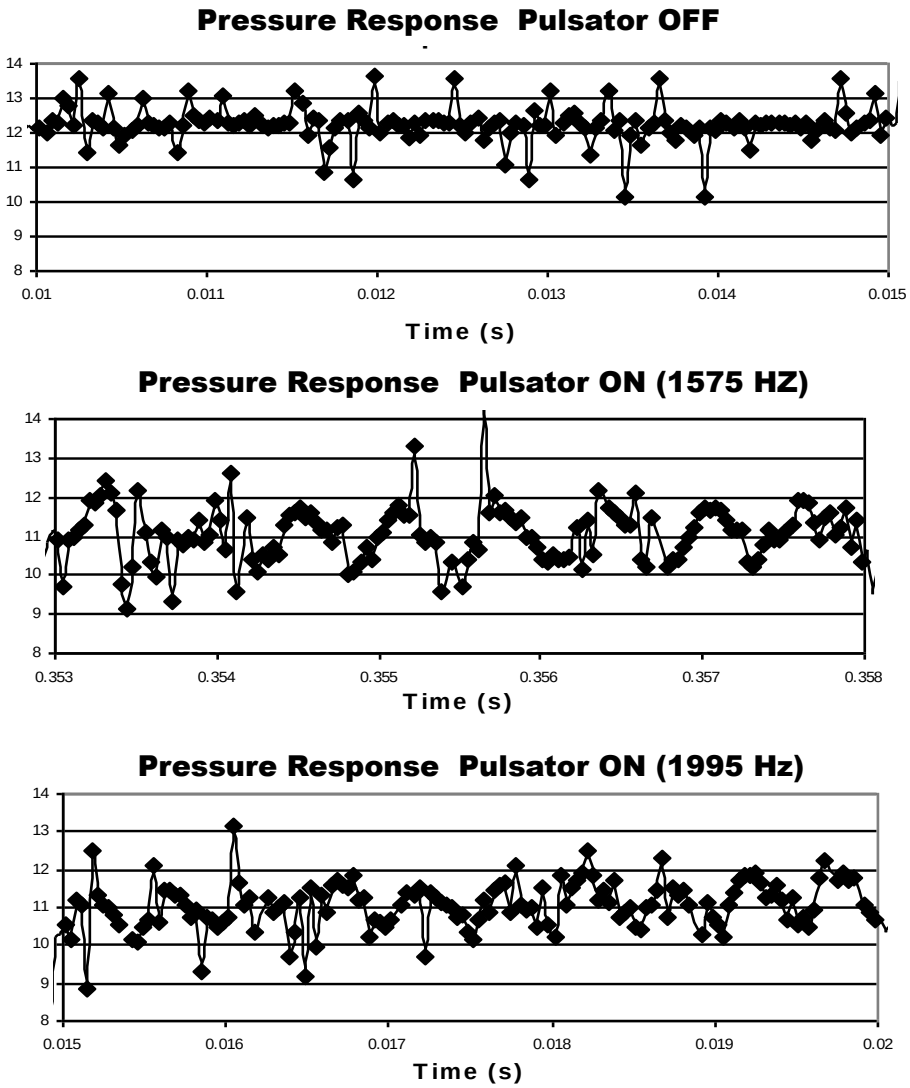

Figure 3.5: Comparison of flow response from high frequency pressure transducer at low pressure.

have a dominant effect on the outputs. As a result the test range was limited to the values used in the CFD modeling to reduce the test matrix size.

The pulsator did develop the desired changes in the feed line pressure. An example from each test is compared in Figure 3.5. The differences can be seen between the noise level with the pulsator off and the oscillation when the pulsator was on.

When the pulsator was turned off, the amplitude is almost constant with little noise. When it was on, the waveform can be seen clearly in the graphs at both motor speeds 75 Hz and 95 Hz. When the pulsator was on, there were some large noise spikes that can be seen on the graphs, but they are not significant to the overall data. The frequencies for each test varied slightly, but were within 3% of the expected value when the data was run though the FFT. There was only one peak after removing the DC shift effects close to 0 Hz. The rest of the spectrum showed little noise and the single dominate frequency was at the pulsator's frequency. There still remains a DC offset issue with the output from the high frequency pressure transducer. The lingering DC offset may be an issue with the dynamic transducer signal. The charge building on the quartz crystal in the transducer may have a DC offset during testing. When the charge on the crystal is not discharged fast enough, the charge builds creating the DC offset.

3.4.3 Orifice Throttle Control

The orifice throttle was designed to be the primary pulsation magnitude control. The orifice throttle control valve has a total range of 3.67 turns. The throttle range is broken up in to 60 degree increments. The throttle position is referenced as a percentage open of the total throttle range.

During an initial round of testing, the entire range of the orifice throttle was investigated. The investigation determined the range that the orifice throttle has an effect on the outputs. During the preliminary testing, it was observed that the frequency response was not affected by the throttle control. The injector pressure

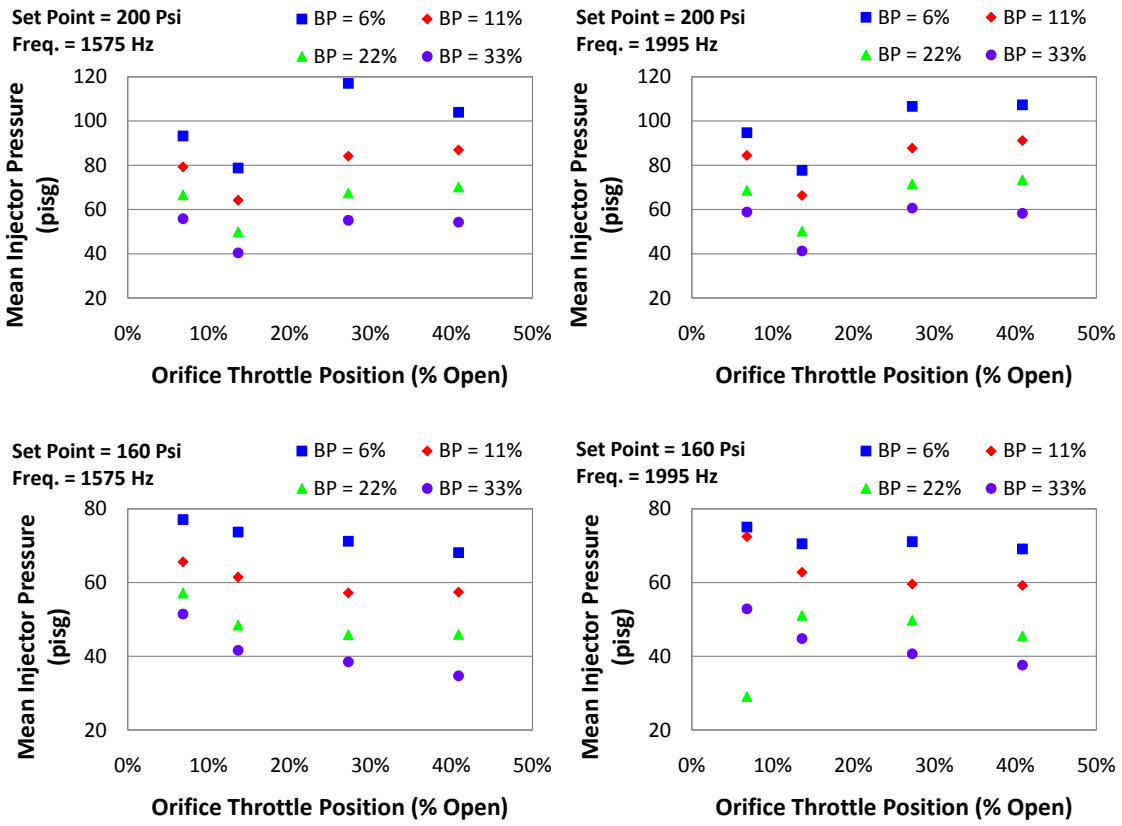

Figure 3.6: Effect of the orifice throttle on injector pressure.

magnitude was affected by the throttle over a range of 0 to 54.5% open; beyond 54.5% open, the orifice throttle had little to no effect. The waste fluid mass flow levelled off and was approximately steady above 31.4% open. After evaluating the results from initial testing, the effective range testing the orifice throttle was set. The characterization testing used values ranging from 6.8% to 31.4% open. Zero turns was not included in the test matrix. The zero position closes off flow entirely, and simulant is required for lubricating and cooling the orifice disk to prevent seal and orifice plate damage.

Figure 3.6 shows the orifice throttle's impact on the mean injector pressure at various back pressure throttle positions. When the pulsator was activated, the original mean injector pressure dropped by 50%. This drop was consistent for both motor frequencies and both pressure set points. At the higher pressure set points, the injector pressure dropped and then recovered as the throttle was opened. The recovery can be seen in Figure 3.6 between 13.6% and 27.3% in the 200 psi graphs. At both lower pressure set points, the pressure continuously dropped as the throttle was opened. The low pressure set points exhibit logarithmic behavior. Curve fitting algorithms produced logarithmic functions with $R^2 > 0.9$. The logarithmic functions predictive capabilities are unsatisfactory because the pattern does not hold across the frequency range. The ineffectiveness of linear, logarithmic and exponential functions to describe the patterns suggests that the geometry has a dominate role in the relationship between the orifice position and injector pressure.

Figure 3.7 shows the throttle position effects on the injector mass flow rates. The first noticeable characteristic is that the data follow the same pattern as the feed line pressure. In a normal injector test, the pressure determines the mass flow. Even though mass flow may be diverted through the pulsator, the feed line pressure determines the mass flow rate through the injector and the pulsator. Attempting to use curve fitting to find functions to describe and predict the mass low behavior was unsatisfactory, just as in the injector pressure results. The mass flow changed by 30% between the highest and lowest mass flow rates. At the low pressure setting, the mass flow rate change is significantly smaller suggesting the throttle control becomes less effective at lower pressures.

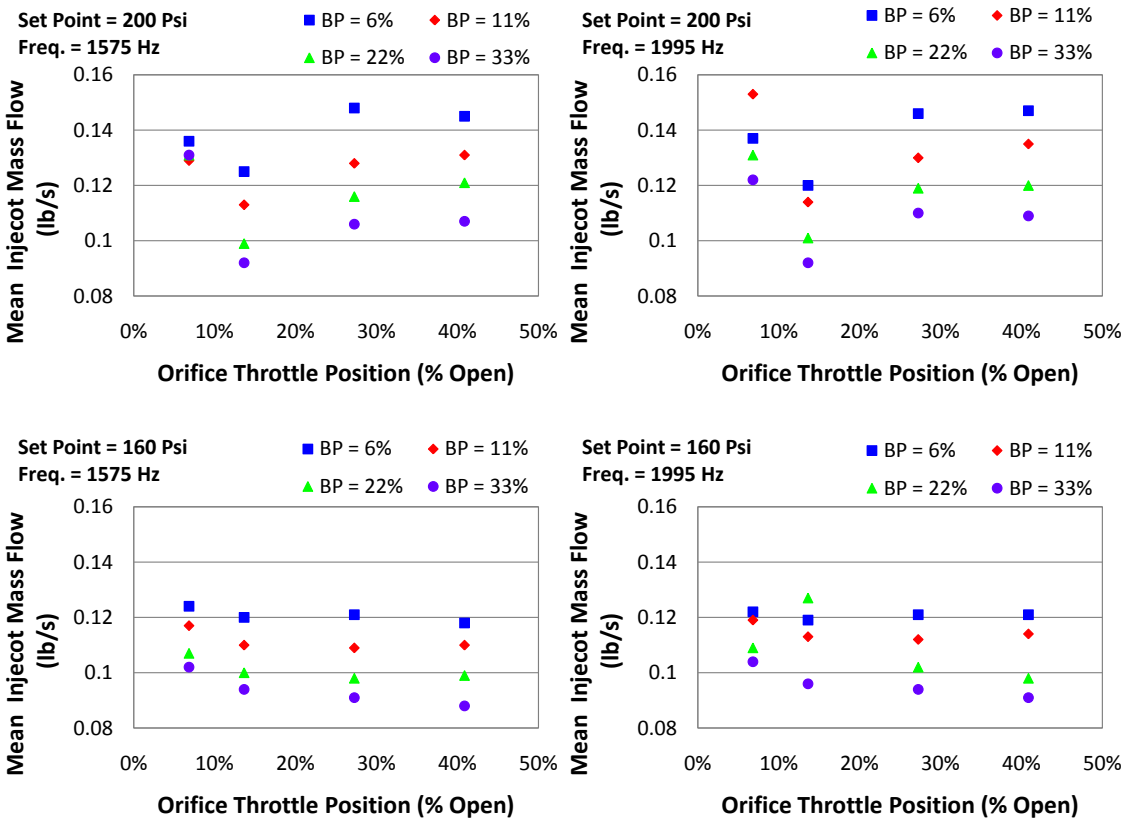

Figure 3.7: Effect of the orifice throttle on injector mass flow.

Figure 3.8 shows the orifice throttle effects on the pulsation amplitude relative to the feed line pressure. The amplitude was taken as the average peak to peak amplitude from multiple data sets at the same set point. This average was divided by the pressure at the injector to give the injector pressure pulsation percentage. The data indicated that the pulsation amplitude decreased with increased throttle position; however, the mean pressure at the injector also decreased. As can be seen in Figure 3.8, the pulsation amplitude relative to the injector pressure increased with increasing the throttle position. The pulsation magnitude does drop, but the feed line pressure drops faster creating an increase in the percent pulsation. The predictive

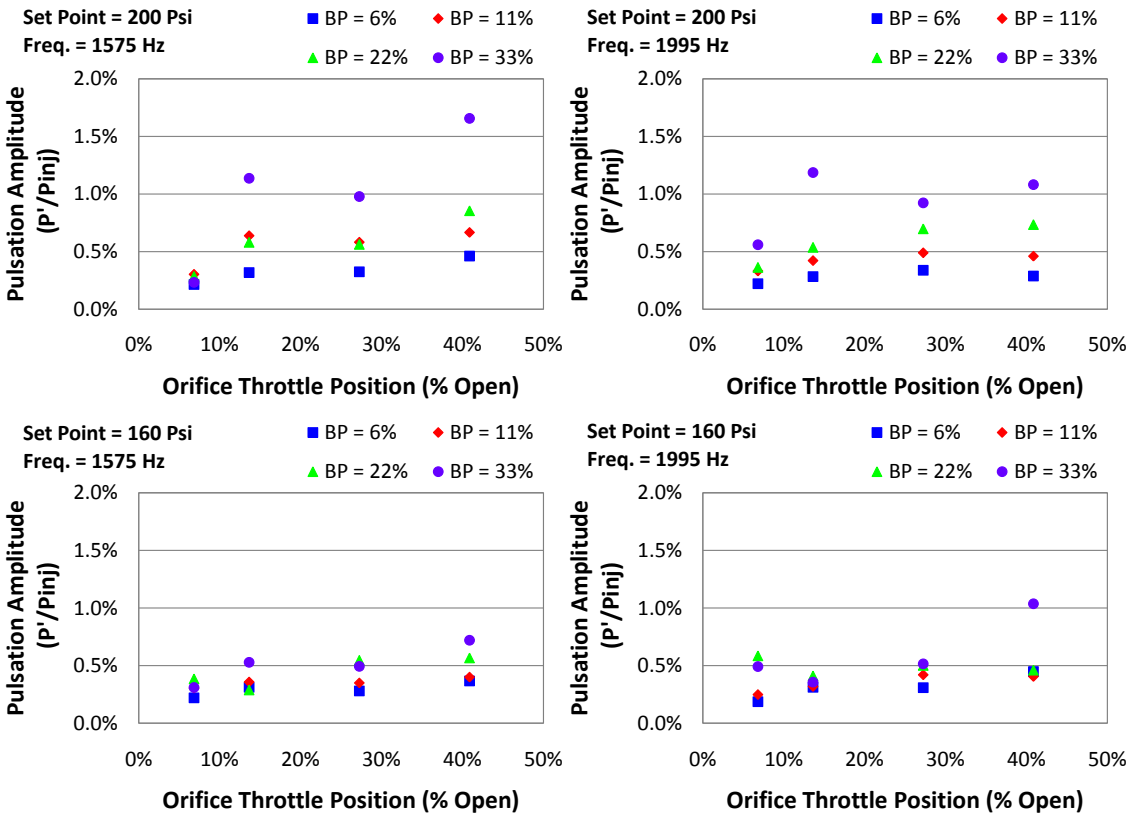

Figure 3.8: Effect of the orifice throttle on percent pulsation.

functions generated from curve fit algorithms still provided limited benefits. Although limited, the use of a linear fit does highlight the back pressure affects. The slope changed in conjunction with the back pressure throttle position. The 200 psi, back pressure throttle 33% open, and orifice throttle 13.6% open data points produce jumps in pulsation. The data points represent synergies in the pressure pulsation response. Even at the maximum pulsation, the pulsation is still an order of magnitude below the desired pulsation amplitude, 10%. The largest pulsation achieved for these test conditions was 2%. This amplitude may not be sufficiently large to simulate the effects of high frequency combustion instability. Higher feed line pressures are

expected to generate larger pressure pulsations. Decreasing the pressure drop across the injector while maintaining the same pressure drop across the orifice plate will increase pulsation. In order to decrease pressure drop across the injector and maintain the pressure drop across the rotating orifice plate, the environment the injector sprays into must be increased above the discharge cavity pressure.

3.4.4 Back Pressure Throttle Control

The pulsator back pressure throttle controls the waste water chamber pressure. The back pressure throttle was a needle valve with a total range of 9 turns and was broken down into 180 degree intervals. The preliminary testing found that only the first 55.6% turns significantly affect the output parameters. As the back pressure throttle was closed, the resistance through the waste line increased, thus the waste water chamber pressure or back pressure increased. The increasing back pressure should reduce cavitation across the orifice disk and decrease the pulsation magnitude by restricting the waste water flow. During testing it was found that the increased back pressure had an adverse side effect. The high back pressure increased the leakage around the rotating shaft seals. The back pressure throttle position's effect on the injector pressure is shown in Figure 3.9 and the mass flow rate is shown in Figure 3.10. As the throttle was opened, the pressure at the injector decreased and consequently the mass flow to the injector also decreased.

Note that in the 200 psi tests the mass flow initially decreased. It was observed during testing that the mass flow came from the seal weep and not the waste water line. As the back pressure was reduced, the amount of fluid lost through the seal

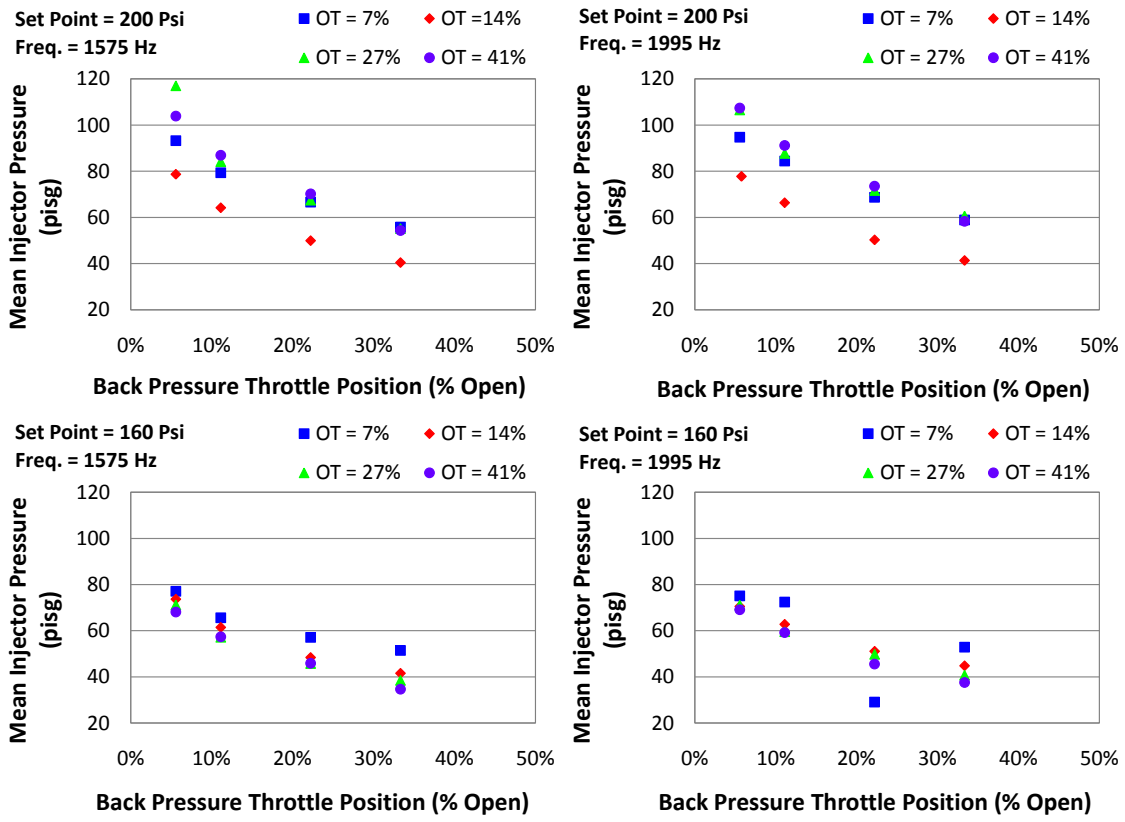

Figure 3.9: Effect of the back pressure throttle on injector pressure.

decreased. The fluid loss through the seals is small at 200 psi, but could become a major concern as the pressure rises and the seals eroded.

The backpressure exhibits the same 50% pressure drop observed in the orifice results. Opening the needle valve reduces the back pressure, resulting in a 80% drop in the mean injector pressure. Figure 3.9 shows that the drop in mean injector pressure is present in all the tests. The drop rate in injector mean pressure is not constant. The response is drastically different from the orifice throttle graphs because of the pressure drop uniformity. Out of the 16 tests, only one of the throttle positions does not have a pressure drop between each test point. The reduction in back pressure

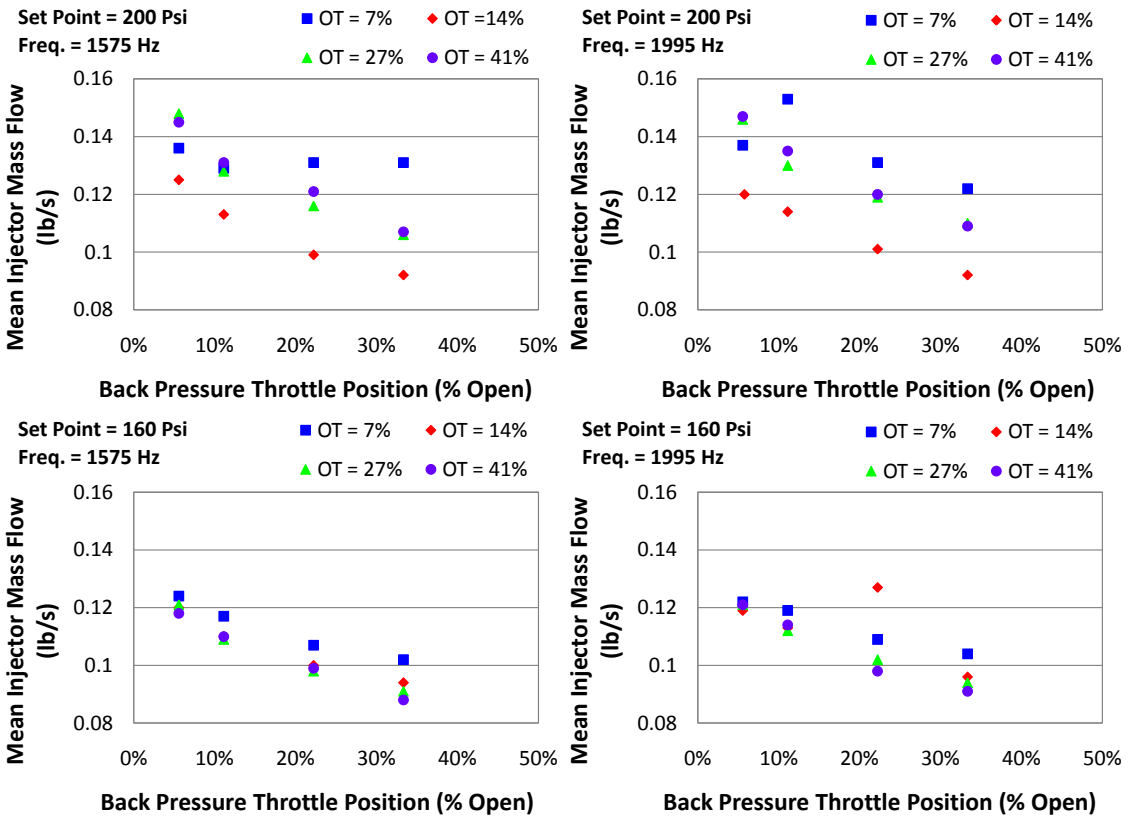

Figure 3.10: Effect of the back pressure throttle on injector mass flow.

throttle and orifice throttle position acts cumulatively to reduce the mean injector pressure. The back pressure throttle has a greater effect than the orifice throttle on the mean injector pressure. The back pressure throttle is capable of changing the mean injector pressure by 25%. The back pressure throttle is the primary control for adjusting the mean injector pressure at a fixed run tank pressure.

The back pressure throttle significantly effects the mass flow rate in the low pressure test where the venturi was not used. The mass flow changed significantly between different initial pressure data sets. The back pressure throttle affects the injector mass flow fraction more than the total mass flow rate. The maximum injector

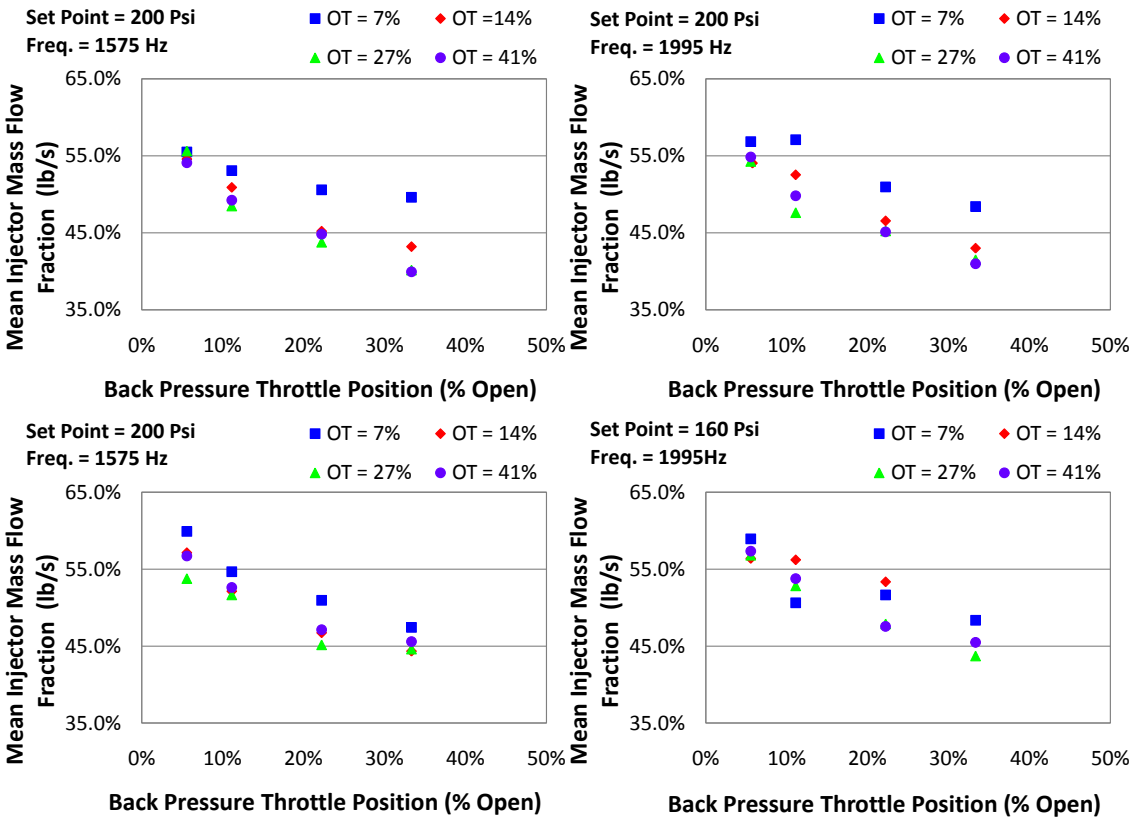

Figure 3.11: Effect of the back pressure throttle on injector mass flow fraction.

flow rate occurs when the back pressure value is at the lowest value 9.1% open. After the back pressure throttle is 11.1% open, the mass flow drops and the waste line mass flow increases. The mass flow to the injector was not the greatest at the highest back pressure due to the amount of water lost through the weep port from leaking seals. The large simulant volume lost through the seal at high pressures may decrease the injector mass flow rate reproducibility at high pressures. In Figure 3.10 the total change in injector mass flow is significantly larger in the 200 psi tests. In the 200 psi pressure tests, the total range of mass flow increases when the orifice throttle position increases. The total mass flow across all tests averaged 0.23 lb/s with a standard

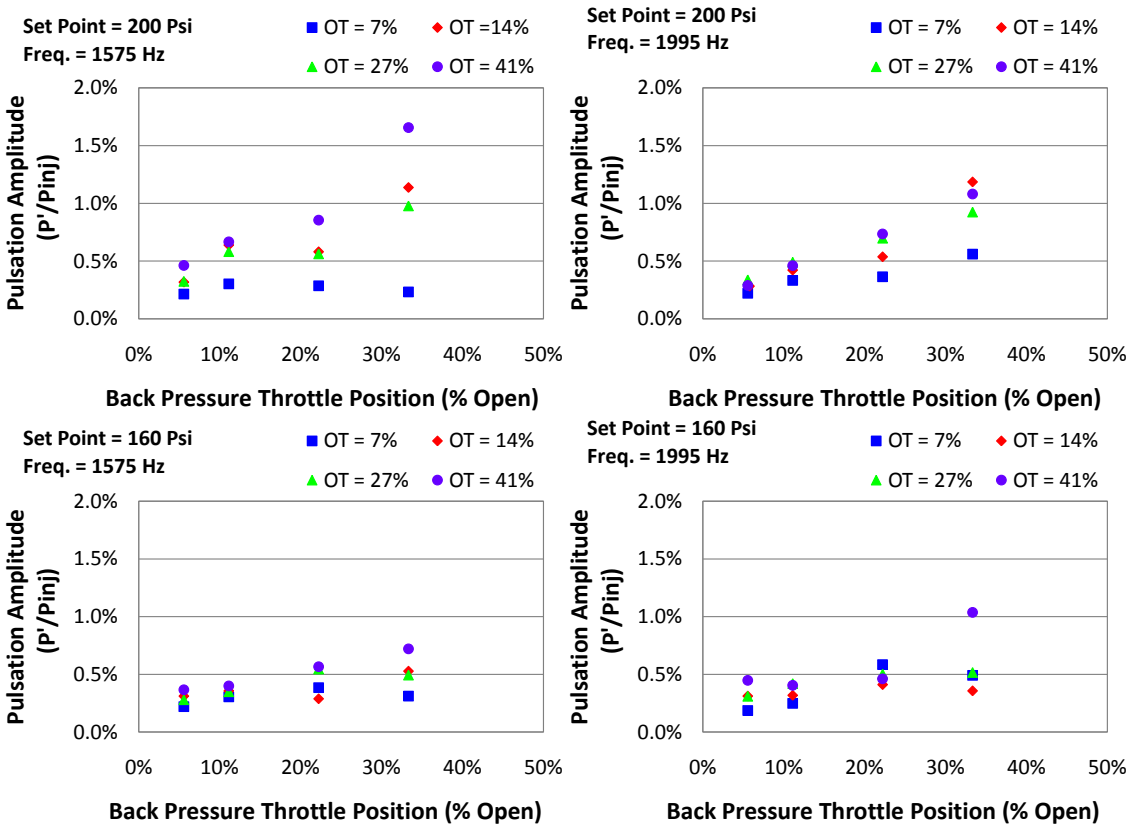

Figure 3.12: Effect of the back pressure throttle on percent pulsation.

deviation of 10%. The injector mass flow fraction decreases as the back pressure throttle is opened. The decreasing mass flow trend can be seen for all the tests in Figure 3.10. The injector mass flow fraction is shown in Figure 3.11. The plots show the injector mass flow fraction ranges from 40% to 60% across all the tests. Based on pulsator design, the waste water mass flow fraction was expected to be 67%. The low pressure test conditions may be reducing the operational mass flow fraction. Because the waste mass flow generates the pressure pulsations, the high injector mass flow fractions produce low pulsations. The mass flow fraction is also not constant between the frequency graphs requiring adaptation between frequency tests.

The back pressure throttle position effect on pulsation amplitude is shown in Figure 3.12. The pulsation magnitude increases relative to the mean injector pressure as the back pressure throttle is opened. The same trend was shown in the percent pulsation versus throttle position in Figure 3.6. The trend confirms the expected results, but it was not expected that there would be data points where pulsation would decrease when the throttle is opened further. In general, lower back pressure throttle positions decrease the injector mass flow fraction, but the decrease in the injector mass flow fraction leads to larger pulsation. As the back pressure throttle is opened, the pulsation amplitude drops because of the drop in the feed line and mean injector pressure; however, the drop in feed line pressure is faster than the drop in pulsation magnitude, resulting in higher percent pulsation. The data show that as the back pressure throttle is opened, a significant increase in pulsation occurs between the first and last test points. The percent pulsation increases two to three times. Injector research often focuses on pulsation as a feed line pressure percent, but magnitude is also important. To maximize pulsation, it is necessary to open the orifice and back pressure throttles. The open throttles lower the pressure leading to low pulsation. Future testing should show the possibilities of increasing pulsation by increasing the feed line pressure. At higher feed line pressures, trade offs will still have to be made between injector mass flow fraction, pulsation amplitude, and feed line pressure.

3.5 High Pressure Characterization

The high pressure characterization was limited in scope because of time constraints and the unexpected damage caused by the pulsator effects on pressure trans-

ducers. The pulsator has four control variables. The tests examine the effects for three variables. The first tests and comparisons recreate the low pressure data graphs. One of the key differences between the low and high pressure characterizations is the method for controlling pressure. During the low pressure tests, the run tank pressure controlled the system pressure; during the high pressure tests, a venturi and run tank pressure controls the total mass flow rate. The higher mass flow rate creates a higher pressure in the system. The amount of data collected increased. The mass flow from the seals and waste fluid line are measured separately, and the data capture rate has been increased to 100 kHz. The values for the test points have changed because the scanning method was used to determine the throttle set points for each frequency. The data from orifice throttle, back pressure throttle, and frequency were examined to determine the influence on the pulsator's output. During the characterization testing, some of the pressure data was concluded to be bad or was not taken because of damage to the pressure transducers. The magnitude of pulsation produced by the pulsator and the number of cycles during tests caused the static transducers to fail. The transducer failures limited the pressure data collected and the size of the test matrix.

3.5.1 Orifice Throttle Control

The throttle control was designed to be the primary method to adjust the pulsation magnitude. The orifice throttle control valve has a total range of 3.67 turns broken down into 60 degree increments. During the initial scan tests, the entire spectrum was scanned to determine the pulsation magnitude inflection points. The

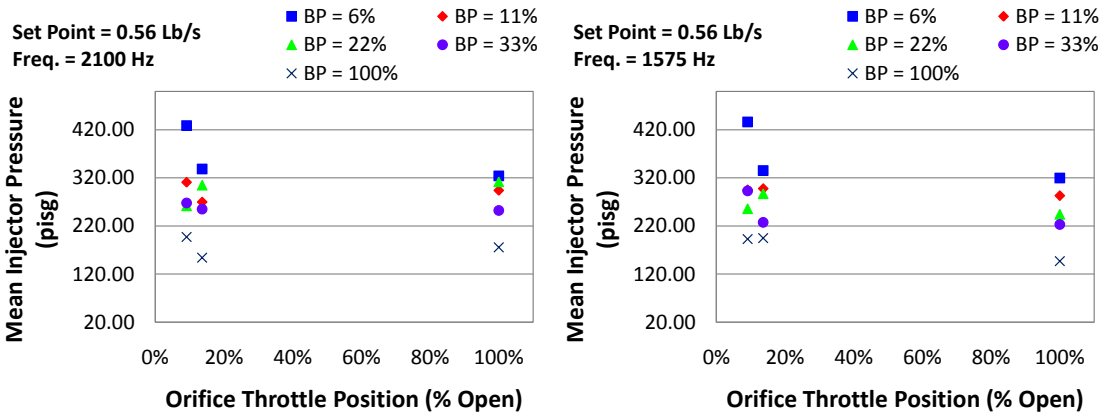

Figure 3.13: Effect of the orifice throttle on injector pressure.

inflection points were then used as the set points for the orifice throttle. The fully open is added to be last test point in the test series. Zero was not used as a data point because the pulsator requires fluid flow to cool and lubricate the rotation orifice disk.

The orifice throttle causes the mean injector pressure to drop. In Figure 3.13, the change in mean injector pressure between frequencies tests is close to zero. The 2100 Hz and 1575 Hz tests have different test points for the first two values, because they were determined from the initial scan. The pressure does not change significantly from the second to third data points. These results reinforce the data from the low pressure test. The low pressure test only used values at the lower end of the throttle range, because the effect of the upper throttle range was determined to be insignificant. The different back pressure throttle positions created similar results with the exception of when the back pressure throttle was set to 44.4% open. At 44.4% open, the injector magnitude starts low and increases at the second data point and decreases to the last data point. The pattern occurs in both frequencies' set

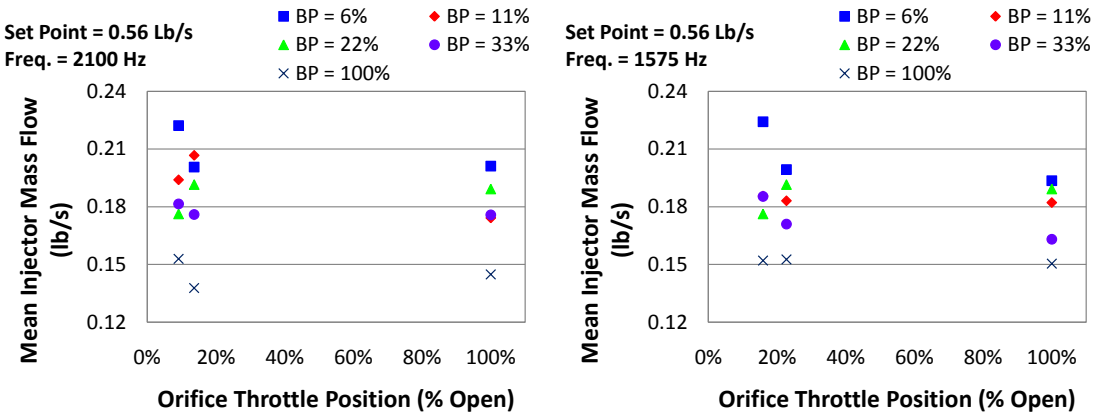

Figure 3.14: Effect of the orifice throttle on injector mass flow.

points. The inconsistency with the pattern at that particular data point is unknown and assumed to be a negative synergy point. Both frequencies cover the same pressure range, 200 to 430 psi. The pressure range increased greatly from the low to the high pressure test.

The mass flow charts in Figure 3.14 are almost identical to the injector pressure data. Only two data points do not match, one from each frequency data set. The data point with the back pressure throttle 19.4% open, the orifice throttle 15.9% open, and 1575 Hz is higher than it should be compared to the data point with the orifice throttle 22.7%. The irregular 2100 Hz data point is the point with the back pressure throttle 11.1% open and the orifice throttle 9.1% open. The data point is above instead of below the next data point.

The percent pulsation graphs, Figure 3.15, do not have clear patterns. The 1575 Hz graph shows an increase in the pulsation as the back pressure throttle is opened. Some of the back pressure settings have increases and decreases in pulsation. The 2100 Hz data shows increases in pulsation from the middle point to the

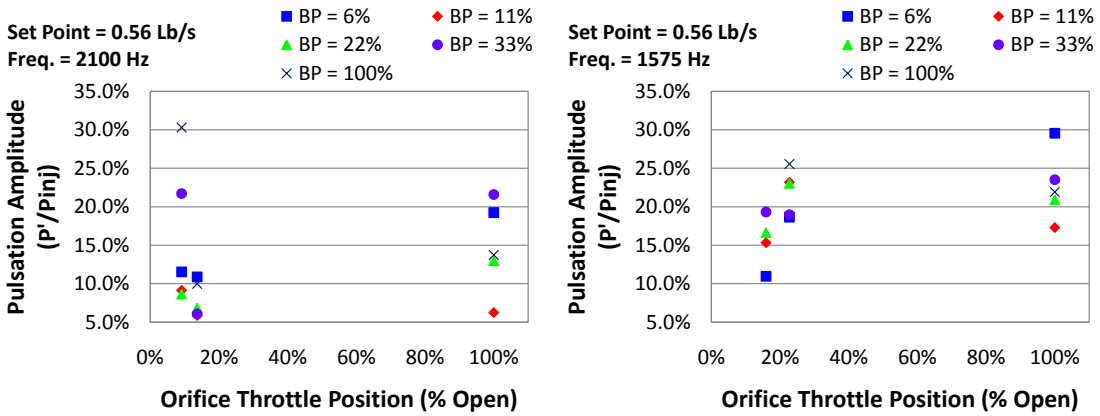

Figure 3.15: Effect of the orifice throttle on percent pulsation.

last point. Between the first and second data point there are small changes, large jumps, increases, or decreases. The unpredictable behavior will make it very difficult to get the desired pulsation magnitudes. The previous graphs of the mean values, Figure 3.13 and Figure 3.14, have significantly less uncertainty than the pulsation data, Figure 3.15. The orifice throttle provides control of the mass flow rate, but does not reliably control pulsation. The lower frequency shows that the uncertainty may be a function of frequency. The consistency in the 1575 Hz pulsation is higher than than the data from the 2100 Hz tests.

3.5.2 Back Pressure Throttle Control

The back pressure throttle controls the waste water chamber pressure. The back pressure throttle is a needle valve with a total range of 9 turns in 180 degree increments. Preliminary testing was performed by scanning through and finding the inflection points similar to the orifice throttle tests. The scanning did not provide any useful data for limiting the test matrix size. Changes were difficult to see on

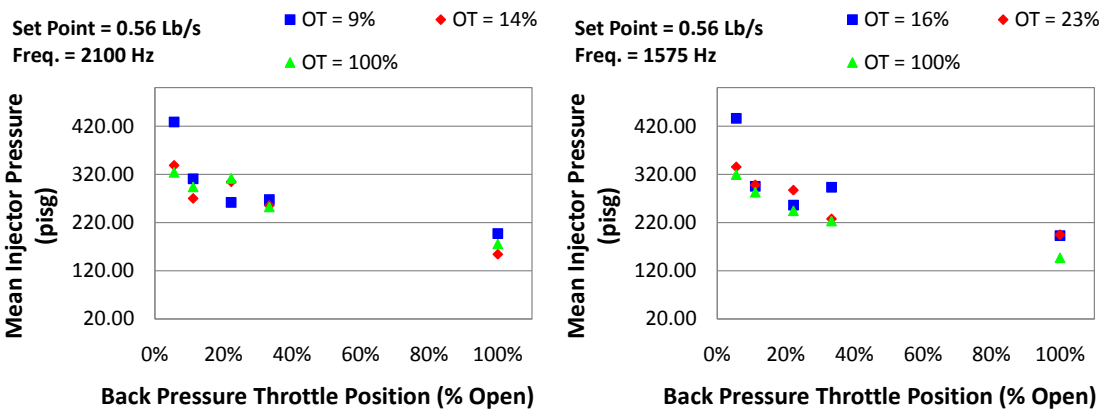

Figure 3.16: Effect of the back pressure throttle on injector pressure.

the oscilloscope. Thus, the same data points were used for the high and low pressure testing. The maximum position was added to the data set to match the orifice throttle data range. Back pressure data shows similar results to the orifice throttle data.

The back pressure throttle has a greater influence on the mean injector pressure flow than the orifice control. The data in Figure 3.16 show that the pressure drop is similar to the low pressure data and the orifice data. The high and low pressure data has the same shape and covers a greater pressure range than the orifice throttle control. The back pressure throttle can change the pressure by 225 psi, more than the entire range of the low pressure data. Compared to the orifice throttle data, the back pressure control is not as smooth and has some jumps in the data. The difference between the orifice and the back pressure controls suggests that the back pressure throttle is a better for course corrections and the orifice throttle is a better fine control for the injector mass flow rate.

Similar to the orifice throttle mass flow data, Figure 3.17 correlates well to the the pressure data Figure 3.16. The mass flow follows the same pattern. The 2100 Hz

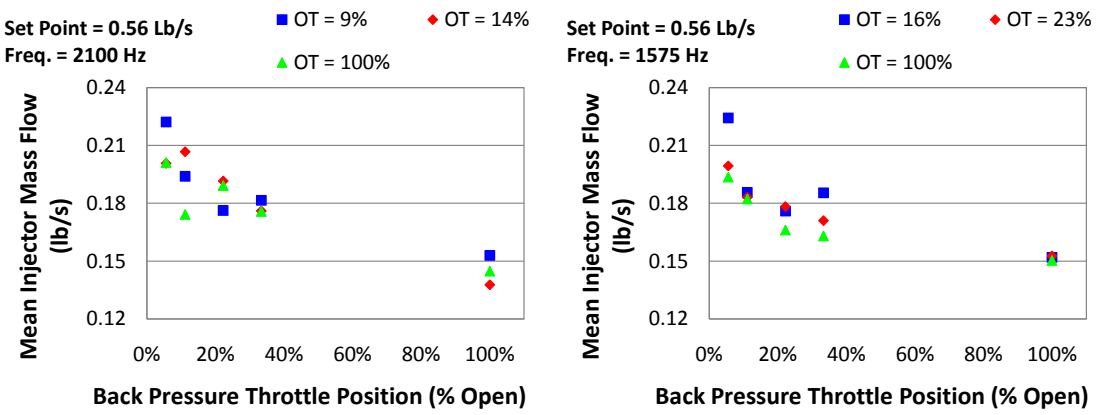

Figure 3.17: Relationship between the feedline pressure and the injector mass flow rate.

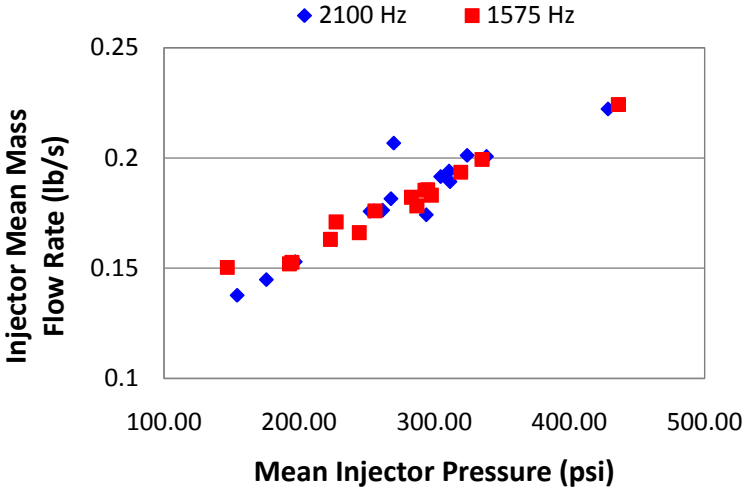

Figure 3.18: Effect of the back pressure throttle on injector mass flow rate.

tests almost overlay each other. The 1575 Hz data has similarities to the orifice throttle pressure data, but does not line up as well as the 2100 Hz data. Figure 3.18, shows a linear relationship between the mean injector pressure and the mass flow rate. The linear relationship is similar to an injector's discharge coefficient. An injector's discharge of coefficient is the relationship between mass flow rate and the square root of the pressure. Sections of the function can appear linear, so the linear relationship could be the injectors discharge coefficient, but more testing is required

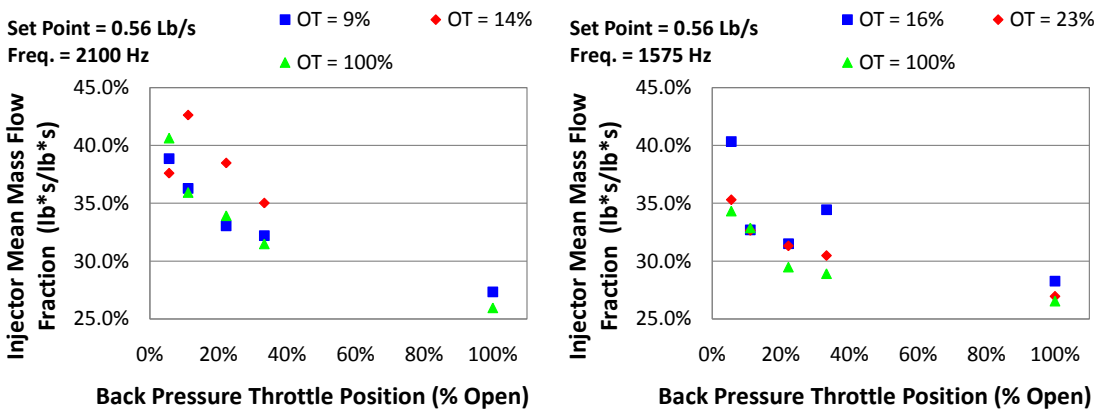

Figure 3.19: Effect of the back pressure throttle on injector mass flow fraction.

to confirm the hypotheses. For testing purposes, the pressure mass flow relationship is sufficiently accurate using as few as four data points. The injector mass flow rate can be controlled using the feed line pressure while the pulsator is on.

The injector mass flow fraction graphs, Figure 3.19, show the same patterns as the injector mass flow data and the injector pressure data. Unlike the previous data, the orifice throttles are not in sequence from top to bottom, the middle orifice throttle position generates the largest mass flow fraction for the 2100 Hz tests. The injector mass flow fraction reduction is caused by the seal leaks. The 1575 Hz data agrees more with expectations. It has the expected patterns with the exception two data points at the first orifice throttle position tests. The mass flow fraction meets the design expectations. Most of the data points have a mass flow fraction in the 30% to 35%, the design calls for a 33% injector mass flow fraction. The volume of waste simulant does cause problems for running long duration tests, because of the total volume of the run tank and the additional uncertainty caused by refilling the run

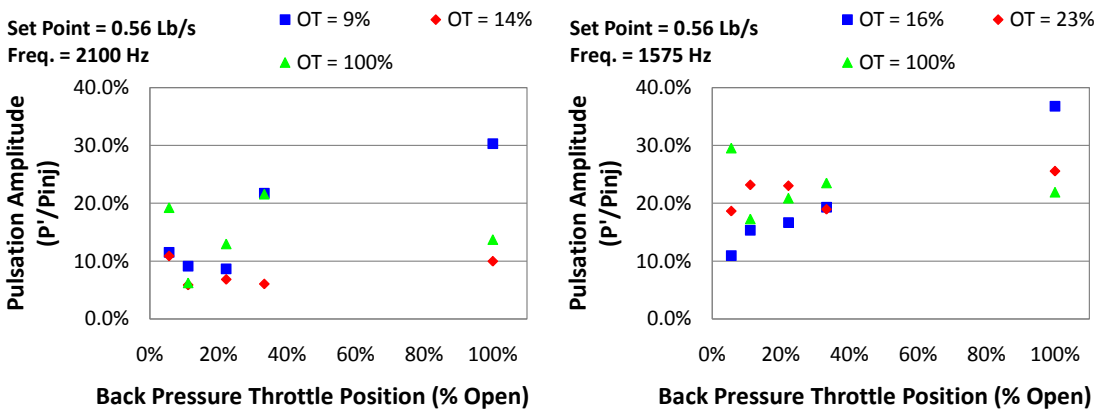

Figure 3.20: Effect of the back pressure throttle on percent pulsation.

tank. The tests run during the characterization ran for less than two minutes per set point.

The pulsation amplitude graphs, Figure 3.20, are similar to the orifice pulsation graphs. There are small patterns within the data sets. None of the patterns fits across the entire spectrum. The 2100 Hz and orifice throttle open 9.1% data starts with a decay pattern for the first three data points. It then jumps to more than twice the pulsation. The middle three data points for 2100 Hz and orifice throttle 18.1% open data have an increasing pulsation trend. The first and last data points do not match the pattern. The patterns are better for the 1575 Hz data. The data with the orifice throttle 15.9% open show a steady increase. It is the only data set that shows a regular pattern. The second set of data with the orifice throttle 22.7% open has higher pulsation at high back pressures, but unexpectedly has a lower maximum pulsation amplitude. The data suggests that the injector pressure drops as the back pressure is opened. The pulsation also increases while opening the back pressure throttle. The low pressure data show that they both decayed with the injector pressure dropping

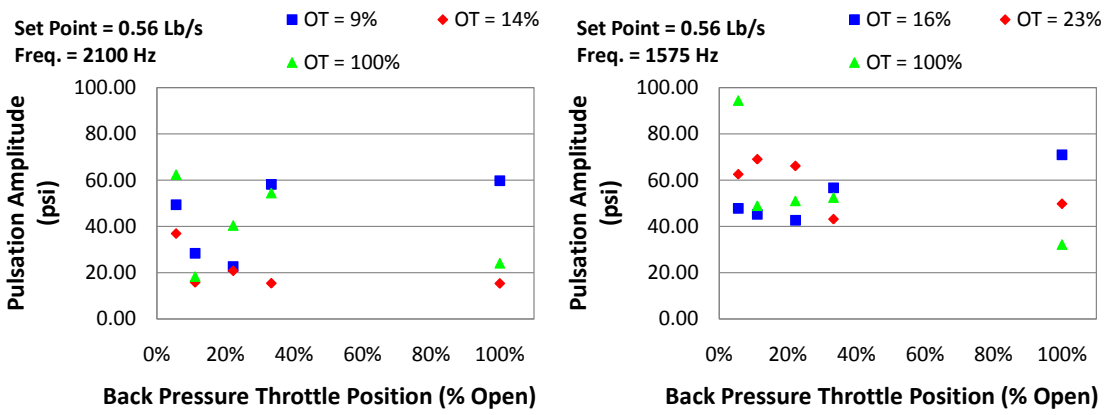

Figure 3.21: Effect of the back pressure throttle on percent pulsation.

faster than the pulsation amplitude. In the previously mentioned data in Figure 3.15, the function of pulsation is related to the throttle position, but it is difficult to distinguish patterns. In Figure 3.21, the magnitude of pulsation also fails to produce patterns. Shifting from percent pulsation to the magnitude of pulsation, the magnitude increases as the back pressure throttle is closed because of the higher system pressure. The magnitude of pulsation is impressive. The lack of patterns highlights the difficulties to set specific pulsation magnitudes or percentages. Controlling the pulsation is a balance between the orifice and back pressure throttles. The pulsation magnitude is greatest when the orifice and back pressure are at opposite ends of their ranges. In the pulsation graphs, the high orifice throttle conditions and low back pressure generate the highest pulsation in both graphs. The second highest pulsation is at the lowest orifice condition and the highest back pressure setting.

3.6 Pulsator Tuning

The characterization data provided the information to develop a method to tune the pulsator to generate specific outputs. The pulsator can then be used in injector testing. The tuning of the pulsator is an iterative process to find the specific set points for an injector test. The first step in the process is to define the relationship between the mass flow rate and the mean injector pressure pressure. The mass flow rate for the venturi should be set to three time the desired flow rate. Four tests should then be conducted including different frequencies and throttle conditions. More tests could be conducted to increase the accuracy of the mass flow pressure relationship. Find the equation for the mass flow rate as a function of injector pressure. Then calculate the pressure necessary to achieve the desired mass flow rate. The initial goal will be to maximize the pulsation first then adjust it as necessary. Set the orifice throttle to 9.1% open. Start the flow and the pulsator. While the pulastor is running, adjust the back pressure to obtain the desired feed line pressure. Opening the back pressure throttle decreases the feed line pressure. After finding the back pressure setting, record data and measure the mass flow rate. If the back pressure throttle is set above 33.3% open, adjust the throttle to change to pulsation. If the back pressure throttle is set below 33.3% open, set the throttle to 100% open. Repeat the process of setting the back pressure throttle. The mass flow and pulsation magnitude should be rechecked. The back pressure can be used to fine tune the pulsation magnitude. The pulsator can be used in injector tests spraying into a pressurized environment. The mass flow can be calculated from the weep and waste mass flow rate. The mass

flow rate may have to be adjusted for several issues. Then at the desired mass flow setting, the pressure across the venturi drop needs to be at least 30%. When the pressure drop is not high enough, the mass flow rate should be reduced or the run tank pressure should be increased and the venturi reset to maintain the original mass flow rate. It is also possible to increase the mass flow rate and decrease the injector mass flow fraction. The decrease in injector mass flow rate generally will result in greater pulsation. Most of the relationships developed are generalizations that may not always hold true. Additional adjustments may have to be made.

CHAPTER 4

CONCLUSIONS

The objective of this study and characterization was to advance utilization of the pulastor to a research tool. The tests evaluated the pulsator's performance and capabilities, so the pulsator could be integrated into current rocket engine research. The pulsator's pulsation response was evaluated in an atmospheric test rig using filtered de-ionized water as the simulant. The pulsator outlet was connected to a swirl injector post to provide downstream flow resistance. Low and high pressure tests were performed. For each test, the time capture methods measured the average waste water, seal leakage, and injector mass flow rates. Dynamic pressure data was recorded at the pulsator exit. The pressure transducers measured the injector, pulsator inlet, and waste water line mean static pressures. Pulsation magnitude, reliability, repeatability, and pulsation effects in the system were examined. The data show that the pulsator is ready for use in injector research. The pulsator has the capability of generating a maximum peak to peak pulsation of 30% at 1575 Hz. The regular appearance of outliers in pulsator results requires additional considerations in the structure of future testing. The dynamic pressure transducer data from different

points in the test facility show that the pulsation diminishes and distorts as pressure waves travel away from the pulsator.

The pulsation test results conclude that the pulsator does generate pressure waves. The pressure waves show up in the dynamic pressure transducer data both in the waveform and the FFT. High speed video demonstrates the pulsation effect on the spray. The repeatability shows significant variation in the pressure waveform and magnitude. The data suggest the problem lies within the second harmonic magnitude and phase shift. The variation is limited to the pressure pulsations. The mean measurements have small uncertainties and high levels of repeatability. The critical mean mass flow rates have uncertainties below 5%.

The detailed characterization studies continued to show the uncertainties in pulsation and complex relationships between the variables. The characterization provides a broad spectrum of data from the entire range of operating capabilities of the pulsator. The characterization demonstrated the ability to generate pressure pulsations over 35% and 100 psi at 1575 Hz and 15% and 60 psi at 2100 Hz . The data provide the basis to build a method to find set points for specific injector tests. The characterization data's results carry the pulsator from the object of research to a research tool.

4.1 Continuing and Future Work

The experimental work successfully established the pulsator capabilities and the possibilities for use in future research. The work can continue in several directions.

The pulsator could be studied to decrease the variation in the pulsation produced. Understanding the second harmonic variation source would be a key first step. Also, the pulsator seals could be redesigned to decrease the seal leaks at high pressures and to decrease wear on the bearings, but the change in fluid flow could change the pulsator response already established.

The test to examine the presence of pulsation indicated, the pulsator frequency test range could be increased dramatically. The pulsator could operate at frequencies as low as 105 Hz. The pulsation magnitude uncertainty decreases between 2100 Hz and 1575 Hz, and at low frequencies the uncertainty may be lower. Injector testing could extend to examining the effects of frequencies in a higher chug instability range.

The pulsator and atmospheric facility is ready to test specific injectors. In particular, attempts could be made to correlate PDPA data with the pulsation frequency. Spray imaging studies could be started using high speed video or strobe imaging. The pulsator and facilities development required significant investment and has many possible applications in future research.

APPENDICES

APPENDIX A

DATA SUMMARY TABLES

Table A.1: Data Recorded During the Tests

Test Number	PSI	Frequency	Orifice	BP	Initial Im	Initial Dm	Initial Wm	I time	D time	W time	I mass	D mass	W mass	File name
D1	700	2100	2	1	0.345	0.363	0.361	20.44	16.00	15.38	4.89	2.20	3.97	detail1
D2	700	2100	2	2	0.349	0.364	0.362	21.59	20.94	15.38	4.54	3.40	3.37	detail2
D3	700	2100	2	4	0.350	0.370	0.369	20.98	15.07	15.38	4.05	3.33	2.84	detail3
D4	700	2100	2	6	0.348	0.372	0.367	14.75	16.97	15.94	3.03	4.63	2.46	detail4
D5	700	2100	2	18	0.391	0.371	0.369	22.82	13.78	100.00	3.88	5.97	0.37	detail5
D6	700	2100	3	1	0.350	0.372	0.371	20.53	15.53	15.66	4.47	2.03	3.92	detail6
D7	700	2100	3	2	0.348	0.365	0.364	20.91	16.75	15.37	4.67	2.00	3.14	detail7
D8	700	2100	3	4	0.350	0.370	0.371	20.57	15.53	15.43	4.29	2.99	2.49	detail8
D9	700	2100	3	6	0.351	0.375	0.375	20.66	15.37	16.15	3.99	3.76	2.09	detail9
D10	700	2100	3	18	0.352	0.376	0.373	21.00	14.66	100.00	3.24	6.71	0.37	detail10
D11	700	2100	22	1	0.349	0.375	0.372	20.62	20.37	15.60	4.50	2.74	3.15	detail11
D12	700	2100	22	2	0.351	0.377	0.377	20.75	15.78	15.47	3.97	2.89	2.72	detail12
D13	700	2100	22	4	0.354	0.377	0.371	20.37	15.50	15.56	4.21	4.07	2.40	detail13
D14	700	2100	22	6	0.351	0.376	0.371	21.32	15.37	16.84	4.10	4.72	2.06	detail14
D15	700	2100	22	18	0.351	0.371	0.371	20.50	15.32	100.00	3.32	6.70	0.37	detail15
D16	700	1575	3.5	1	0.352	0.376	0.373	21.00	28.06	15.81	5.06	3.92	3.62	detail16
D17	700	1575	3.5	2	0.349	0.373	0.370	20.28	15.34	15.53	4.11	2.73	3.92	detail17
D18	700	1575	3.5	4	0.352	0.374	0.372	19.36	15.46	16.16	3.76	3.48	3.31	detail18
D19	700	1575	3.5	6	0.354	0.379	0.376	20.41	15.37	17.09	4.14	4.16	2.20	detail19
D20	700	1575	3.5	18	0.355	0.381	0.376	20.41	16.19	30.50	3.46	6.54	0.54	detail20
D21	700	1575	5	1	0.351	0.356	0.370	20.34	15.72	15.47	4.41	1.96	4.45	detail21
D22	700	1575	5	2	0.351	0.376	0.374	20.41	15.19	15.57	4.09	2.58	4.00	detail22
D23	700	1575	5	4	0.352	0.374	0.373	20.40	15.50	15.47	3.99	3.50	3.31	detail23
D24	700	1575	5	6	0.349	0.370	0.366	21.16	16.00	15.59	3.97	4.31	2.61	detail24
D25	700	1575	5	18	0.349	0.374	0.370	20.35	15.03	16.31	3.46	6.26	0.73	detail25
D26	700	1575	22	1	0.351	0.370	0.375	16.78	16.09	15.30	3.60	2.05	4.44	detail26
D27	700	1575	22	2	0.352	0.371	0.374	20.28	16.94	15.41	4.05	2.72	3.97	detail27
D28	700	1575	22	4	0.353	0.371	0.374	20.00	16.03	15.47	3.68	3.69	3.31	detail28
D29	700	1575	22	6	0.350	0.371	0.374	20.53	15.96	16.03	3.70	4.21	2.95	detail29
D30	700	1575	22	18	0.351	0.372	0.374	20.00	15.35	17.68	3.36	6.38	0.82	detail30

Table A.2: Mass Flow Calculations

Test Number	Mdot I	Mdot D	Mdot W	Total Mdot	Total M Error
D1	0.222	0.115	0.235	0.572	4.0%
D2	0.194	0.145	0.196	0.535	-2.8%
D3	0.176	0.196	0.161	0.533	-3.0%
D4	0.181	0.251	0.131	0.564	2.5%
D5	0.153	0.407	0.000	0.560	1.7%
D6	0.201	0.107	0.226	0.534	-3.0%
D7	0.207	0.098	0.181	0.485	-11.8%
D8	0.192	0.169	0.138	0.498	-9.5%
D9	0.176	0.220	0.106	0.503	-8.6%
D10	0.138	0.432	0.000	0.569	3.5%
D11	0.201	0.116	0.178	0.495	-10.0%
D12	0.174	0.159	0.152	0.485	-11.8%
D13	0.189	0.238	0.131	0.558	1.4%
D14	0.176	0.282	0.100	0.558	1.5%
D15	0.145	0.413	0.000	0.558	1.4%
D16	0.224	0.126	0.206	0.556	1.1%
D17	0.186	0.153	0.229	0.568	3.2%
D18	0.176	0.201	0.182	0.559	1.6%
D19	0.185	0.246	0.107	0.538	-2.1%
D20	0.152	0.380	0.006	0.538	-2.2%
D21	0.199	0.102	0.264	0.565	2.7%
D22	0.183	0.145	0.233	0.561	2.0%
D23	0.178	0.201	0.190	0.569	3.5%
D24	0.171	0.246	0.144	0.561	2.0%
D25	0.153	0.391	0.022	0.566	3.0%
D26	0.194	0.104	0.266	0.564	2.5%
D27	0.182	0.139	0.233	0.554	0.8%
D28	0.166	0.207	0.190	0.563	2.4%
D29	0.163	0.240	0.160	0.564	2.5%
D30	0.150	0.391	0.025	0.567	3.0%

Table A.3: System Pressure Values

Test Number	Sys P	Sys STDEV	Runtank	RT STDEV	Venturi	Venturi STDEV
D1	1640.39	37.98	694.97	28.79	676.09	20.51
D2	1048.88	11.01	654.01	25.36	637.81	19.36
D3	880.11	9.52	659.77	25.35	642.47	19.06
D4	1643.66	35.27	651.56	26.65	638.43	17.71
D5	1637.02	34.90	690.70	26.33	675.14	18.12
D6	1230.53	9.94	655.86	24.43	639.90	17.00
D7	1845.05	36.53	685.74	29.72	664.81	21.98
D8	1845.99	34.78	682.49	28.22	662.84	19.45
D9	1850.19	35.74	676.14	28.48	655.64	20.96
D10	1853.30	35.97	680.36	28.76	660.07	21.01
D11	1860.87	37.03	663.80	29.14	649.33	22.30
D12	1863.56	38.09	676.85	29.77	663.07	22.64
D13	1873.12	38.18	654.99	29.79	642.05	21.91
D14	1872.11	37.64	659.28	29.39	647.65	21.13
D15	1642.44	35.89	669.69	27.09	655.53	18.13
D16	1862.74	37.46	668.53	29.21	649.21	19.95
D17	1642.78	42.41	676.85	32.41	661.83	23.78
D18	1641.83	38.44	682.17	28.83	667.79	18.90
D19	1861.31	37.50	675.33	29.35	655.27	19.83
D20	1862.34	38.09	669.48	29.48	651.61	20.46
D21	1637.69	34.96	690.95	26.01	677.40	17.17
D22	1636.41	35.93	695.57	26.97	681.73	18.60
D23	1636.15	35.61	692.10	26.61	677.29	18.04
D24	1626.16	34.16	669.18	26.60	649.03	16.94
D25	1625.46	34.16	659.14	26.34	638.97	16.49
D26	1624.40	37.25	679.78	28.60	658.14	19.93
D27	1622.78	35.78	678.99	27.89	656.30	18.67
D28	1621.29	35.08	677.78	27.34	655.58	17.71
D29	1619.43	34.13	689.10	26.08	666.48	16.69
D30	1617.82	36.70	691.77	28.29	671.14	18.84

Table A.4: Data Relating to Pulsator Operation

Test Number	Input P	Input STDEV	Output	Output STDEV	Waste P	Waste STDEV	DeltaP	Pulse %
D1	430.28	18.49	428.60	10.05	-1.47	5.39	49.38	11.5%
D2	316.39	19.15	310.91	9.24	186.85	7.01	28.39	9.1%
D3	267.39	20.48	261.74	8.88	129.72	6.59	22.62	8.6%
D4	270.74	24.71	267.89	8.70	-1.53	4.99	58.20	21.7%
D5	201.08	25.53	197.04	8.89	-2.42	4.95	59.71	30.3%
D6	344.79	18.33	338.64	8.21	246.13	6.66	36.89	10.9%
D7	271.67	20.27	269.96	9.70	180.79	6.65	15.85	5.9%
D8	306.59	17.92	304.70	9.38	222.93	6.63	20.84	6.8%
D9	257.35	19.43	255.23	9.62	168.61	6.38	15.45	6.1%
D10	155.89	21.10	154.01	9.46	15.00	6.19	15.37	10.0%
D11	331.63	16.36	324.29	10.19	267.96	6.80	62.42	19.2%
D12	299.04	20.86	294.05	10.48	232.90	6.97	18.36	6.2%
D13	325.56	8.54	311.60	10.27	198.13	7.23	40.45	13.0%
D14	240.51	8.72	252.44	10.61	149.44	7.07	54.47	21.6%
D15	178.82	28.22	175.65	8.85	-2.44	5.09	24.11	13.7%
D16	502.05	25.61	436.21	9.78	348.04	6.63	47.76	10.9%
D17	298.72	24.26	295.10	11.96	-1.60	5.40	45.22	15.3%
D18	260.26	21.17	256.08	9.25	-1.55	4.85	42.64	16.7%
D19	265.01	12.75	293.13	9.94	141.55	6.69	56.64	19.3%
D20	-53.53	21.91	192.81	10.36	17.30	6.96	70.91	36.8%
D21	336.93	24.09	335.28	9.87	-1.58	4.85	62.52	18.6%
D22	299.62	25.67	297.78	10.35	-1.58	5.14	69.02	23.2%
D23	289.53	16.20	287.09	12.67	-1.54	5.04	66.12	23.0%
D24	230.23	19.43	227.34	8.27	-1.56	4.84	43.10	19.0%
D25	198.37	17.38	194.61	8.15	-2.46	4.71	49.75	25.6%
D26	322.79	24.18	319.59	10.20	-1.53	4.81	94.42	29.5%
D27	287.59	23.28	283.06	10.35	-1.53	5.05	48.94	17.3%
D28	248.98	19.31	244.45	8.76	-1.59	5.01	51.04	20.9%
D29	227.89	18.54	223.16	8.51	-1.59	4.78	52.48	23.5%
D30	148.48	13.54	146.84	9.85	-2.44	5.13	32.18	21.9%

APPENDIX B

MATLAB CODE

```
clear all
%import data file
filename='position5.txt';


waveheight=20; fftheight=10;
%variables to control set graph sizes

%import data from data file
R = importdata(strcat('Data\',filename), '\t',0);

%seperate out the data from the header
currentdata=R;

%Isolate the high freq. data
%convert from voltage to psi
highfreq=18.7126*(currentdata(:,5));



%Size of FFT also the sample rate
NFFT = (length(highfreq));
B = fft(highfreq,NFFT)/(length(highfreq));

%create frequency range
f = NFFT/2*linspace(0,1,NFFT/2+1);

% Create a single-sided amplitude spectrum.
%abs, makes it single sided
%2*, is adding the other side back sides are symmetrical
```

```
Y=2*abs(B(1:NFFT/2+1));

%remove any DC signal
highfreq=highfreq-real(B(1));

%%%%%%%%%%%%%%%%%%%%%%%%%%%%%%%%%%%%%%%%%%%%%%%%%%%%%%%%%%%%%%%%%%%%%%%%%%%%
% The Following Code is in sections to make different types of graphs
%%%%%%%%%%%%%%%%%%%%%%%%%%%%%%%%%%%%%%%%%%%%%%%%%%%%%%%%%%%%%%%%%%%%%%%%%%%%
%One Combo Graph
    h=figure('position', [1 500 900 350]);
    figure(h)
    clf('reset')

    % Create axes
    axes1 = axes('Parent',figure(h),...
    'Position',[0.07 0.15 0.52 0.76],...
    'FontName','Times New Roman','Fontsize',14);
    % Set X and Y the axis limits
    xlim(axes1,[0 .01]);
    ylim(axes1,[-waveheight waveheight]);
    box(axes1,'on');
    hold(axes1,'all');

    % Create plot
    plot((0:.00001:.01),highfreq(1500:2500),'Parent',axes1);
    title(strcat('Pressure Pulsation of Data File [',filename,']'))
    % Create xlabel
    xlabel('Time(s)','FontName','Times New Roman','Fontsize',14);
    % Create ylabel
    ylabel('P-Mean P (psi)','FontName','Times New Roman',...
    'Fontsize',14);
    hold off

    axes2 = axes('Parent',figure(h),...
    'Position',[0.67 0.15 0.30 0.76],'FontName','Times New Roman',...
    'Fontsize',14);

    % Set X and Y the axis limits
    xlim(axes2,[0 5000]);
    ylim(axes2,[0 fftheight]);
    box(axes2,'on');
    hold(axes2,'all');

    plot(f(1:5000),Y(1:5000),'Parent',axes2)
    title('Waveform Frequencies','FontName','Times New Roman',...
```

```
    'Fontsize',14)
    xlabel('Frequency (Hz)','FontName','Times New Roman',...
    'Fontsize',14)
    ylabel('Component Apliude (psi)','FontName','Times New
      Roman','Fontsize',14)
%-------------------------------------------------------------------%

%%%%%%%%%%%%%%%%%%%%%%%%%%%%%%%%%%%%%%%%%%%%%%%%%%%%%%%%%%%%%%%%%%%
%  %Large Pulsation Graph
%  %The following code creates a figure with only a large waveform graph
%      h=figure('position', [1 550 965 400]);
%      figure(h)
%      clf('reset')
%
%      % Create axes
%      axes1 = axes('Parent',figure(h),...
%      'FontName','Times New Roman');
%
%    % Set X and Y the axis limits
%      xlim(axes1,[0 .01]);
%      ylim(axes1,[-40 40]);
%      box(axes1,'on');
%      hold(axes1,'all');
%
%      %Create plot
%      plot((0:.00001:.01),highfreq(1000:2000),'Parent',axes1);
%      title(strcat('Pressure Pulsation of Data File [',filename,']'))
%      % Create xlabel
%      xlabel('Time(s)','FontName','Times New Roman');
%      % Create ylabel
%      ylabel('P-Mean P (psi)','FontName','Times New Roman');
%      hold off
%
% %Large FFT Graph
% %The following Code creates a figure with a single large FFT graph
%      h=figure('position', [1 50 965 400]);
%      figure(h)
%      clf('reset')
%
%      % Create axes
%      axes1 = axes('Parent',figure(h),...
%      'FontName','Times New Roman');
%      % Set X and Y the axis limits
%      xlim(axes1,[0 5000]);
%      ylim(axes1,[0 20]);
```

```
%      box(axes1,'on');
%      hold(axes1,'all');
%
%      plot(f(1:5000),Y(1:5000),'Parent',axes1)
%      title('Frequency of High Frequency Pressure Transducer')
%      xlabel('Frequency (Hz)')
%      ylabel('Component Apliude (psi)')
%      hold off
%-------------------------------------------------------------------%

%%%%%%%%%%%%%%%%%%%%%%%%%%%%%%%%%%%%%%%%%%%%%%%%%%%%%%%%%%%%%%%%%%%%%%
%  %Small Pulsation Graph
%  %The following code creates a figure with a single small
%  %waveform graph
%      h=figure('position', [1 550 550 375]);
%      figure(h)
%      clf('reset')
%
%      % Create axes
%      axes1 = axes('Parent',figure(h),...
%      'FontName','Times New Roman');
%      % Set X and Y the axis limits
%      xlim(axes1,[0 .01]);
%      ylim(axes1,[-40 40]);
%      box(axes1,'on');
%      hold(axes1,'all');
%
%      % Create plot
%      plot((0:.00001:.01),highfreq(1000:2000),'Parent',axes1);
%      title(strcat('Pressure Pulsation of Data File [',filename,']'))
%      % Create xlabel
%      xlabel('Time(s)','FontName','Times New Roman');
%      % Create ylabel
%      ylabel('P-Mean P (psi)','FontName','Times New Roman');
%      hold off
%
% %Small FFT Graph
% %The following code creates a figure with a single small FFT graph
%
%      h=figure('position', [1 50 550 375]);
%      figure(h)
%      clf('reset')
%
%      % Create axes
%      axes1 = axes('Parent',figure(h),...
```

```
%      'FontName','Times New Roman');
%      % Set X and Y the axis limits
%      xlim(axes1,[0 5000]);
%      ylim(axes1,[0 20]);
%      box(axes1,'on');
%      hold(axes1,'all');
%
%      plot(f(1:5000),Y(1:5000),'Parent',axes1)
%      title('Frequency of High Frequency Pressure Transducer')
%      xlabel('Frequency (Hz)')
%      ylabel('Component Apliude (psi)')
%      hold off
%-------------------------------------------------------------------------%

%this exclueds frequencies under 50 Hz from the max
index=find(Y==max(Y(50:50001)));

%find first peak above 2 psi this should be the
%frequency of the pulsator
frequency=find(Y(100:2500)>2,1)+100;


%number of data points in 1.25 cycles based on FFT rounded up
%this is the window size
n=ceil(10^5*1.25/frequency);
%number of windows in data set rounded down
cycles=floor(10^5/n);

% %initalize varibles
 runningmaxavg=0;
 runningminavg=0;
%
for i = 1:cycles

    %find the maximum in each cycle
    index2=find(highfreq((n*(i-1)+1):(n*i))==
        max(highfreq((n*(i-1)+1):(n*i))))+n*(i-1);

    %include the point before and after to reduce effect of noise on
        result
  runningmaxavg=runningmaxavg+highfreq(index2(1))+highfreq(index2(1)+1);
    if index2(1)==1
    %cannot have index value of zero if max is first value use first
            value twice
        runningmaxavg=runningmaxavg+highfreq(index2(1));
```

```
      else
        runningmaxavg=runningmaxavg+highfreq(index2(1)-1);
    end

    %find the minimum in each cycle
    index2=find(highfreq(n*(i-1)+1:n*i)==
       min(highfreq(n*(i-1)+1:n*i)))+n*(i-1);

%include the point before and after to reduce effect of noise on result

  runningminavg=runningminavg+highfreq(index2(1))+highfreq(index2(1)+1);
   if index2(1)==1    %cannot have index value of zero if max is first
                      %value use first value twice
        runningminavg=runningminavg+highfreq(index2(1));
    else
        runningminavg=runningminavg+highfreq(index2(1)-1);
    end

end

%calculate the average considering the 3 data point from each cycle
averagedeltaP=(runningmaxavg-runningminavg)/(3*cycles);

%Show peak to peak pulsation in command window
display(averagedeltaP);


% Impose sine wave over wave form to compare results

% figure(1)
% hold on;
% t=linspace(0,300/10^5,300);
%  %plot(Y(index)*sin(2*pi*t*transpose(f(index))),'r')
%  %adds sin wave to graph with FFT max value
%  %plot(AmpRMS*sin(2*pi*t*transpose(f(index))),'r');
%  %adds sin wave to graph with RMS amplitude
% hold off;


%Output results to file

%Mean and Stdev of System pressure
%Mean and Stdev of Liquid Sim Venturi
%Mean and stdev of Run Tank
%Mean and stdev of High Frequency Pressure
```

```
%Mean and stdev of Pulsator Input
%Mean and stdev of Pulsator Output
%Mean and stdev of Pulsator Waste
DataAverage=mean(currentdata);
DataStdev=std(currentdata);

Alldata=[DataAverage(2), DataStdev(2), DataAverage(4), DataStdev(4),
  DataAverage(3), DataStdev(3), DataAverage(6), DataStdev(6),
  DataAverage(7), DataStdev(7), DataAverage(8), DataStdev(8),
  DataAverage(5), DataStdev(5), averagedeltaP ];

save('figuredata.txt','Alldata', '-ASCII', '-tabs','-append')
```

REFERENCES

[1] Khil, T., Kim, S., Cho, S., and Yoon, Y., "Quantification of the Transient Mass Flow Rate in a Simplex Swirl Injector," *Measurement Science and Technology*, Vol. 20, No. 7, 2009, pp. 075405–075414.

[2] Ahn, B., *Forced Excitation of Swirl Injectors using a Hydro-Mechanical Pulsator*, Purdue University Master's Thesis, West Lafayette, IN, 2009.

[3] Harrje, D. and Reardon, F., "Liquid Propellant Rocket Combustion Instability," Tech. Rep. NASA SP-194, National Aeronautics and Space Administration, Washington, DC, 1972.

[4] Culick, F. and Yang, V., "Overview of Combustion Instabilities in Liquid-Propellant Rocket Engines," *Liquid Rocket Engine Combustion Instability*, edited by V. Yang and W. Anderson, Progress in Astronautics and Aeronautics, American Institure of Astronautics and Aeronautics, 1995, pp. 3–37.

[5] United States Government, "Budget of the United States Government, Fiscal Year 2011," United States Office of Management and Budget, United States Government Printing Office, 2010.

[6] Hulka, J. R., "Scaling of Performance in Liquid Propellant Rocket Engine Combustion Devices," *AIAA Joint Propulsion Conference*, No. 2008-5113, American Institute of Aeronautics and Astronautics, Hartford, CT, 2008.

[7] Sutton, G. P. and Biblarz, O., *Rocket Propulsion Elements*, John Wiley & Sons, New York, 7th ed., 2001.

[8] Cavitt, R., *Experimental Methodology for Measuring Combustion and Injection Coupled Responses*, UAHuntsville Master's Thesis, Huntsville, AL, 2007.

[9] Byrd, R., *Laboratory Scale Injector Instability Mode Assessment*, UAHuntsville Master's Thesis, Huntsville, AL, 2008.

[10] Kenny, R., *Influence of variable Thrust Parameters on Swirl Injector Fluid Mechanics*, UAHuntsville Ph.D Dissertation, Huntsville, AL, 2008.

[11] Rhy, N., *Acoustic Excitation and Destruction of Liquid Sheets*, UAHuntsville Ph.D Dissertation, Huntsville, AL, 2009.

[12] Hoover, D., Ryan, H., Pal, S., Merkle, C., Jacobs, H., and Santoro, R., "Pressure Oscillation Effects on Jet Breakup," *Heat and Mass Transfer in Spray Systems*, Heat Transfer Division, American Society of Mechanical Engineers, 1991.

[13] Ghafourian, A., McGuffin, R., Mahalingam, S., and Daily, J., "Dynamic Response to Acoustic Perturbation of an Atomizing Coaxial Jet in Liquid Rocket Engine," *AIAA Aerospace Sciences Meeting*, No. 93-0232, American Institute of Aeronautics and Astronautics, Reno, NV, 1993.

[14] Ivett A. Leyva, B. C. and Tally, D., "Dark Core Analysis of Coaxial Injectors at Sub-, Near-, and Supercritical Pressures in a Transverse Acoustic Field," *AIAA Joint Propulsion Conference*, No. 2007-5456, American Institute of Aeronautics and Astronautics, Cincinnati, OH, 2007.

[15] Davis, D. W. and Chehroudi, B., "Shear-Coaxial Jests from a Rocket-like Injector in a Transverse Acoustic Field at Hight Pressures," *AIAA Aerospace Sciences Meeting*, American Institute of Aeronautics and Astronautics, Reno, NV, 2006.